

# **Gamma-rays and Neutrinos from Cosmic Accelerators**



# Contents

<b>1</b>	<b>Topics</b>	<b>5</b>
1.1	ICRANet participants . . . . .	5
1.2	Ongoing collaborations . . . . .	5
<b>2</b>	<b>Brief description</b>	<b>7</b>
<b>3</b>	<b>Publications-2013</b>	<b>9</b>
3.1	Publications-2007-2012 . . . . .	9
<b>4</b>	<b>On the gamma-ray emission from the core and radio lobes of the radio galaxy Centaurus A</b>	<b>11</b>
4.1	Introduction . . . . .	11
4.2	The core of Cen A . . . . .	12
4.2.1	Spectral Analysis . . . . .	13
4.3	Temporal Variability . . . . .	15
4.4	Discussion and Conclusion-1 . . . . .	16
4.5	The lobes of Cen A . . . . .	20
4.5.1	Spatial analysis . . . . .	20
4.5.2	Spectral analysis . . . . .	23
4.6	The origin of the non-thermal lobe emission . . . . .	24
4.6.1	Inverse-Compton origin of $\gamma$ -rays . . . . .	25
4.6.2	Hadronic $\gamma$ -rays? . . . . .	27
4.7	Discussion and conclusion-2 . . . . .	28
<b>5</b>	<b>On the Detectability of High-Energy Galactic Neutrino Sources</b>	<b>31</b>
5.1	Introduction . . . . .	31
5.2	Using high energy $\gamma$ -rays as a guide for high energy neutrino search . . . . .	32
5.3	Toward reliable predictions for the SNR RX J1713.7-3946 . . . . .	35
5.4	An appraisal of a telescope in the Northern Hemisphere . . . . .	38
5.5	Summary and discussion . . . . .	40
<b>6</b>	<b>Future plans related to the Byurakan Observatory</b>	<b>43</b>



# 1 Topics

- High energy gamma-ray emission from active galactic nuclei
- Galactic sources of high energy neutrinos

## 1.1 ICRA Net participants

- Aharonian Felix
- Harutyunian Haik
- Sahakyan Narek

## 1.2 Ongoing collaborations

- Francesco Vissani (INFN, Gran Sasso Theory Group, Italy)
- Marco Tavani (INAF-IASF Roma and Universit di Roma "Tor Vergata", Italy)
- Frank Rieger (Max-Planck-Institut für Kernphysik, Germany)
- Rui-zhi Yang (Key Laboratory of Dark Matter and Space Astronomy, China)
- Giovanni Piano (INAF-IASF Roma, INFN Roma and Univ. Tor Vergata, Italy)



## 2 Brief description

The works done and currently being developed within our group lie in the field of particle astrophysics including high energy gamma and neutrino astrophysics. The detection of these particles gives the opportunity to understand the physical processes that occur in astrophysical sources: they are not affected by interaction with extragalactic and galactic electromagnetic fields before they reach the Earth, and therefore point directly to the source of emission.

We have been interested in studying High Energy (HE) gamma emission from Active Galactic Nucleus (AGNs) in particular HE emission from Centaurus A (Cen A) radio galaxy/AGN. Cen A is a prototype Fanaroff-Riley Class I Fanaroff and Riley (1974) radio source and as a misaligned BL Lac-type object at higher energies Morganti et al. (1992); Chiaberge et al. (2001), Cen A is known for a complex and extended radio morphology, with two giant outer lobes extending over  $\sim 10^\circ$  and oriented primarily in the north-south direction Feain et al. (2011). Optical images reveal the bright host galaxy bulge ( $\sim 5'$  bulge radius) and the famous, warped dark lane of gas, dust and young stars ( $\sim 12'$  in east-west extension) which obscures the inner part of the galaxy. Chandra X-ray observations show a one-sided, kpc-scale (up to  $\sim 4.5$  kpc in projection) jet composed of several bright knots and diffuse emission, while high-resolution radio VLBI observations have also resolved jet and counter-jet features on sub-parsec scales into discrete components Kraft et al. (2002); Müller et al. (2011). These and related observations suggest that Cen A is a non-blazar source with its jet inclined at a rather large viewing angle  $\gtrsim 50^\circ$  and characterized by moderate (radio) bulk flow speed  $\lesssim 0.5c$  Tingay et al. (1998); Hardcastle et al. (2003); Müller et al. (2011). Its bolometric luminosity of  $L \sim 10^{42}$  erg/s Meisenheimer et al. (2007); van der Wolk et al. (2010), accompanied by indications for the lack of a dust torus, is thought to be powered by gas accretion onto a supermassive black hole of mass  $M_{\text{BH}} \simeq (3 - 12) \times 10^7 M_\odot$  Marconi et al. (2006); Cappellari et al. (2009).

We have studied high energy gamma-ray emission from Cen A radio galaxy in the energy range from 200 MeV to 100 GeV using public available Fermi LAT data.

Furthermore we have been interested in studying HE neutrino emission from astrophysical sources; in some cases HE neutrinos are the only messengers which arrive to the Earth since they do not interact effectively with matter or radiation field unlike the gamma rays. In some sources (for example, in Su-

pernovae Remnants), observed gamma rays can be successfully interpreted either leptonic or hadronic scenarios; therefore the detection (or no detection) of neutrinos is the only way to distinguish between these two possibilities, i.e. hadronic and leptonic models, respectively. The arrival of new HE neutrino detectors like IceCube and KM3NeT will open a new window to understand the physical processes occurring in distance sources. The theoretical estimates of the neutrino fluxes contain large uncertainties and are model dependent, thus it is important formulate the conditions for the detectability of certain neutrino sources phenomenologically (model-independent). In fact, since most galactic neutrino sources are transparent for TeV gamma-rays, their detectability implies a minimum flux of the accompanying gamma-rays. Assuming that the gamma-rays originate from hadronic interactions (pp interaction), we have estimated the flux of gamma-rays assuming a detection of one neutrino per km per year.

## 3 Publications-2013

- Sahakyan, N., Yang, R. Aharonian, F. and Rieger, F., " Evidence for a Second Component in the High-energy Core Emission from Centaurus A?", The Astrophysical Journal Letters, Volume 770, Issue 1, L6.
- Sahakyan, N., Piano, G. and Tavani, M.; "Hadronic Gamma-Ray and Neutrino Emission from Cygnus X-3", The Astrophysical Journal, doi:10.1088/0004-637X/779/1/1.
- Sahakyan, N. and Rieger, F., "On the gamma-ray emission from the core and radio lobes of the radio galaxy Centaurus A", Proc. of HEAPRO IV, will appear in International Journal of Modern Physics: Conference Series

### 3.1 Publications-2007-2012

- Yang, R.-Z., Sahakyan, N., de Ona Wilhelmi, E., Aharonian, F. and Rieger, F., "Deep observation of the giant radio lobes of Centaurus A with the Fermi Large Area Telescope", Astronomy & Astrophysics, 542, A19, 2012.
- Sahakyan, N., "High energy gamma-radiation from the core of radio galaxy Centaurus A", Astrophysics, 55, 14, 2012.
- Sahakyan, N., "On the Origin of High Energy Gamma-Rays from Giant Radio Lobes Centarus A", International Journal of Modern Physics Conference Series, 12, 224, 2012.
- Vissani, F., Aharonian, F. and Sahakyan, N., "On the detectability of high-energy galactic neutrino sources", Astroparticle Physics, 34, 778, 2011.



# 4 On the gamma-ray emission from the core and radio lobes of the radio galaxy Centaurus A

## 4.1 Introduction

The bright, nearby radio galaxy Cen A is the best-studied extragalactic objects over a wide range of frequencies Israel (1998). Its unique proximity ( $d \sim 3.7$  Mpc) and peculiar morphology allow a detailed investigation of the non-thermal acceleration and radiation processes occurring in its active nucleus and its relativistic outflows.

At MeV energies, Cen A has been observed with both OSSE (0.05-4 MeV) and COMPTEL (0.75-30 MeV) onboard the Compton Gamma-Ray Observatory (CGRO) in the period 1991-1995 Steinle et al. (1998). An agreement of the OSSE spectrum with the COMPTEL one in the transition region around 1 MeV, and correlated variability has been found Steinle et al. (1998). At higher energies, a marginal ( $3\sigma$ ) detection of gamma-rays from the core of Cen A was reported with EGRET (0.1-1.0 GeV), but due its large angular resolution the association with the core remained rather uncertain Hartman et al. (1999). Unlike the initial variability (month-type?) seen at lower energies, the flux detected by EGRET appeared stable during the whole period of CGRO observation Sreekumar et al. (1999). At high-energy (HE;  $200 \text{ MeV} < E < 100 \text{ GeV}$ ) Fermi-LAT has recently detected  $\gamma$ -ray emission from the core (i.e., within  $\sim 0.1^\circ$ ) and the giant radio lobes of Cen A (Abdo et al. (2010a,b)): An analysis of the available ten-month data set reveals a point-like emission region coincident with the position of the radio core of Cen A, and two large extended emission regions detected with a significance of 5 and  $8\sigma$  for the northern and the southern lobe, respectively. The HE emission from the core extends up to  $\sim 10$  GeV and is well described by a power-law function with photon index  $\sim 2.7$ . At VHE ( $> 100$  GeV) energies, Cen A has also been detected (with a significance of  $5\sigma$ ) by the H.E.S.S. array based on observations in 2004-2008. The results show an average VHE spectrum compatible with a power law of photon index  $\Gamma = 2.73 \pm 0.45_{stat} \pm 0.2_{syst}$  and an integral flux  $F(E > 250 \text{ GeV}) = (1.56 \pm 0.67_{stat}) \times 10^{-12} \text{ cm}^{-2} \text{ s}^{-1}$  Aharonian et al. (2009). No evidence for variability has been found in the H.E.S.S. data set, but given the weak signal no certain conclusions can be drawn.

i) In the case of the core the apparent lack of significant variability features at GeV and TeV energies has so far precluded robust inferences as to the physical origin of the core emission in Cen A. Unfortunately, the resolutions of current gamma-ray instruments is not sufficient to localize the gamma-ray emitting region(s) either: The angular resolutions of both the H.E.S.S. array ( $\sim 0.1^\circ$ ) and *Fermi*-LAT ( $0.1^\circ$  -  $1^\circ$ , depending on energy) correspond to linear sizes of the gamma-ray emitting region(s) of about 5 kpc or larger. This  $\sim 5$ -kpc-region contains several potential gamma-ray emitting sites such as the central black hole, the sub-pc- or the kpc-scale jet etc. Based on the reported results, one thus cannot distinguish whether the gamma-rays observed from the core in Cen A originate in compact or extended regions. This motivated us to have a new look on the core emission based on four year of *Fermi*-LAT data.

ii) If the extended HE emission from Cen A is generated by indeed inverse-Compton up-scattering of CMB and EBL (extragalactic background light) photons, this could offer a unique possibility to spatially map the underlying relativistic electron distribution in this source. The detection of GeV  $\gamma$ -rays from the radio lobes implies magnetic field strengths  $\lesssim 1 \mu\text{G}$  (e.g., Abdo et al. (2010a)). This estimate can be obtained quite straightforwardly from the comparison of radio and  $\gamma$ -rays, assuming that these radiation components are produced in the same region by the same population of electrons through synchrotron and inverse-Compton processes. In general, however, the radio and the  $\gamma$ -ray region do not need to coincide. While the radio luminosity depends on the product of the relativistic electron density  $N_e$  and the magnetic-field square  $B^2$ , the inverse-Compton  $\gamma$ -ray luminosity only depends on  $N_e$ . This implies that  $\gamma$ -rays can give us model-independent information about both the energy and the spatial distribution of electrons, while the radio image of synchrotron radiation strongly depends on the magnetic field. As a consequence, the  $\gamma$ -ray image can be larger than the radio image if the magnetic field drops at the periphery of the region occupied by electrons. This provides one of the motivations for a deeper study of the extended HE (lobe) emission region in Cen A. We analyze 3 yr of *Fermi* LAT data, increasing the available observation time by more than a factor of three with respect to the previously reported results. The larger data set allows a detailed investigation of the spectrum and morphology of the lobes with better statistics, especially above 1 GeV, where the spectral shape may reflect cooling effects and/or maximum energy constraints on the parent population of particles generating the HE  $\gamma$ -ray emission.

## 4.2 The core of Cen A

For the study of HE emission from the core of Cen A we use publicly available *Fermi*-LAT  $\sim 4$  yr data from 4th August 2008 to 1st October 2012 (MET

239557417–370742403). *Fermi*-LAT on board the Fermi satellite is a pair-conversion telescope designed to detect high-energy  $\gamma$ -rays in the energy range 20 MeV - 300 GeV Atwood et al. (2009). It constantly scans the entire sky every three hours and is always in survey mode although in the past some dedicated pointing observation were done. We use the Pass 7 data and analyze them using the Fermi Science Tools v9r27p1 software package. The entire data set was filtered with *gtselect* and *gtmktime* tools and retained only events belonging to the class 2, as is recommended by the Fermi/LAT science team<sup>1</sup>. To reject atmospheric gamma-rays from the Earth's limb, events with zenith angle  $< 100$  deg are selected. The standard binned maximum likelihood analysis is performed using events in the energy range 0.1–100 GeV extracted from a  $10^\circ$  region centered on the location of Cen A, which is referred to as 'region of interest' (ROI). The fitting model includes diffuse emission components and gamma-ray sources within ROI which are not associated with Cen A (the model file is created based on *Fermi*-LAT second catalog Nolan et al. (2012) and the fluxes and spectral indices are left as free parameters in the analysis. In the model file, the giant radio lobes were modeled using templates from WMAP-k band observation of the source which is extracted from NASA's SkyView. The background was parameterized with the files `gal_2yearp7v6_v0.fits` and `iso_p7v6source.txt` and the normalizations of both components were allowed to vary freely during the spectral point fitting.

### 4.2.1 Spectral Analysis

Initially the continuum gamma-ray emission of the core of Cen A is modeled with a single power law. The normalization and power-law index are considered as free parameters then the binned likelihood analysis is performed. From a binned *gtlike* analysis, the best-fit power-law parameters for the core of Cen A are

$$\left(\frac{dN}{dE}\right)_p = (2.73 \pm 0.12) \times 10^{-9} \left(\frac{E}{100 \text{ MeV}}\right)^{-2.69 \pm 0.03}. \quad (4.2.1)$$

This corresponds to an integral flux of

$$F_\gamma = (1.61 \pm 0.06) \times 10^{-7} \text{ photon cm}^{-2}\text{s}^{-1}, \quad (4.2.2)$$

with only statistical errors taken into account. The test statistic (defined as  $TS = 2(\log L - \log L_0)$ , where  $L$  and  $L_0$  are the likelihoods when the source is included or not) is  $TS = 1978$  above 100 MeV, corresponding to a  $\approx 44 \sigma$  detection significance. The results are consistent with the parameters found in Abdo et al. (2010b), namely photon index  $\Gamma = 2.67 \pm 0.08$  (between 200

<sup>1</sup><http://fermi.gsfc.nasa.gov/ssc/data/analysis/documentation/Cicerone/Cicerone.Data.Exploration/Data.preparation.html>

MeV and 30 GeV) and integral flux  $(1.50 \pm 0.37) \times 10^{-7}$  ph cm $^{-2}$ s $^{-1}$  above 100 MeV (model B). Figure 4.1 shows the spectrum of the core of Cen A obtained by separately running *gtlike* for 12 energy bands, where the dashed line shows the best-fit power-law function for the data given in Eq. (4.2.1). For the highest energy bin (56.2-100 GeV), an upper limit is shown. The spec-

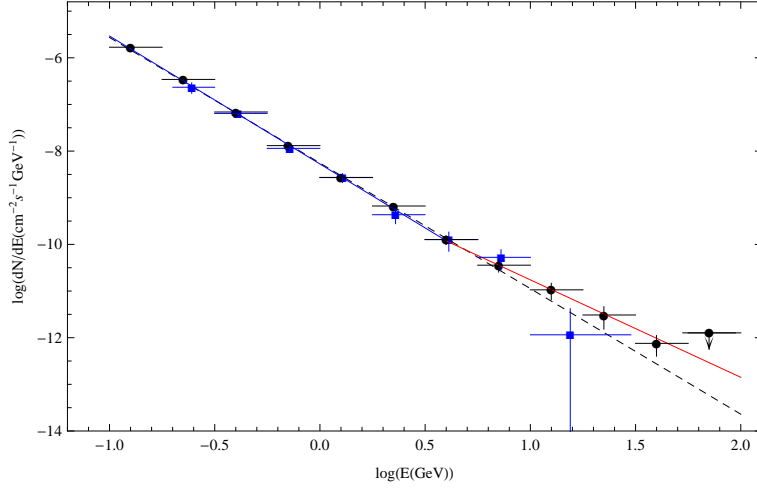


**Figure 4.1:** Average high-energy gamma-ray (>100 MeV) spectrum of the core of Cen A (black points - this work) as compared to the one based on the initial 10 month data set (blue squares - Abdo et al., 2010b). The dashed black line shows the power-law function determined from the *gtlike*. The blue and the red line show power-law fits to the energy bands below and above  $E_b \simeq 4$  GeV, respectively.

trum shows a tendency for a deviation from a single power-law model with respect to the data above several GeV. Indeed, a  $\chi^2$  fit of the power-law model to the data gives a relatively poor fit with  $\chi^2 = 39.7$  for 9 degrees of freedom (dof), and its probability is  $P(\chi^2) < 2 \times 10^{-5}$ . In order to investigate this in more detail, the core spectrum is modeled with a broken power-law model and *gtlike* tool is retried. The best-fit broken power-law parameters are

$$\left(\frac{dN}{dE}\right)_{BP} = (1.19 \pm 0.08) \times 10^{-13} \left(\frac{E}{E_b}\right)^{-\Gamma_{1,2}}, \quad (4.2.3)$$

and

$$F_\gamma = (1.67 \pm 0.06) \times 10^{-7} \text{ photon cm}^{-2}\text{s}^{-1}, \quad (4.2.4)$$

with  $\Gamma_1 = 2.74 \pm 0.02$  and  $\Gamma_2 = 2.12 \pm 0.14$  below and above  $E_b = (4.00 \pm 0.09)$  GeV, respectively. In order to compare the power-law and the broken-power-law model, a log likelihood ratio test between the models is applied. The test statistic is twice the difference in these log-likelihoods, which gives 9 for this case. Note that the probability distribution of the test statistic can be

approximated by a  $\chi^2$  distribution with 2 dof, corresponding to different degrees of freedom between the two functions. The results give  $P(\chi^2) = 0.011$ , which again indicates a deviation from a simple power-law function. The results of the data analysis with a broken power-law model reveal a hardening of the (average) gamma-ray core spectrum towards higher energies. The "unusual" break at 4 GeV could most naturally be explained by a superposition of different spectral components. In order to study this deeper, we divide the data set into two parts, i.e., (0.1- 4) GeV and (4-100) GeV. (Note that the 4 GeV-value is obtained from binned maximum likelihood analyses). The core spectrum of Cen A in both energy ranges is then modeled with a power-law function and the *gtlike* tool is separately applied to these two energy bands. The photon index and flux between 100 MeV and 4 GeV are  $\Gamma_1 = 2.74 \pm 0.02$  and  $F_\gamma = (1.68 \pm 0.04) \times 10^{-7}$  photon  $\text{cm}^{-2}\text{s}^{-1}$ , respectively, and the test statistics gives TS=1944. The result is shown with a blue line in Figure 4.1. On the other hand, for the energy range (4-100) GeV we obtain  $\Gamma_2 = 2.09 \pm 0.2$  and  $F_\gamma = (4.20 \pm 0.64) \times 10^{-10}$  photon  $\text{cm}^{-2}\text{s}^{-1}$ , respectively, and a TS value of 124.4, corresponding to a  $\approx 11 \sigma$  detection significance. This component is depicted with a red line in Figure 4.1. Moreover, to derive the most likely coordinates of the observed gamma-ray emission *gtfindsrc* tool is applied, yielding RA =  $201.387^\circ$ , Dec =  $-43.028^\circ$  with a 95% confidence error circle radius of  $r_{95} = 0.04^\circ$  and RA =  $201.387^\circ$ , Dec =  $-43.028^\circ$  with  $r_{95} = 0.04^\circ$  for energy ranges (0.1- 4) GeV and (4-100) GeV, respectively. This coordinates are offset by  $0.04^\circ$  and  $0.018^\circ$  from the VLBI radio position of Cen A (RA =  $201.365^\circ$ , Dec =  $-43.019^\circ$  Ma et al. (1998)).

### 4.3 Temporal Variability

Variability, if present, could provide important constraints on the emitting region(s). An observed HE flux variation on time scale  $t_{\text{var}}$ , for example, would limit the (intrinsic) size of the gamma-ray production region to  $R' \leq \frac{\delta_D}{1+z} ct_{\text{var}}$  where  $\delta_D$  is Doppler factor and  $z$  is the red-shift. However, previous HE and VHE gamma-ray observations of the core of Cen A with *Fermi*-LAT Abdo et al. (2010b) and H.E.S.S. Aharonian et al. (2009) did not find evidence for significant variability. Here we investigate whether the longer (4 yr) data set employed changes this situation. We thus divide the whole data set (from August 4th 2008 to October 1st 2012) into different time bins and generate light curves using the unbinned likelihood analysis with *gtlike*. Due to limited photon statistics the shortest time scale that one can probe is 15 days. In our analysis we generate light curves in 15, 30, 45 and 60 day bins. The normalization of the core and background point sources are treated as free parameters, but the photon indices of all sources and the normalization of the lobes are fixed to the values obtained in 100 MeV-100 GeV energy range for the whole time period. Since no variability is expected for the underlying

background diffuse emission, the normalization of both background components is fixed to the values obtained for the whole time period. To search

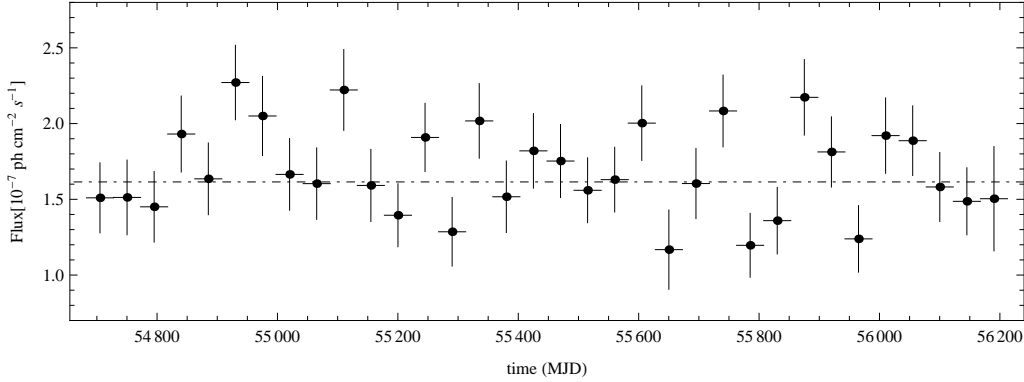


**Figure 4.2:** Gamma-ray light curve from August 4th 2008 to October 1st 2012. The bin size is 45 day. The background diffuse emission (both galactic and extragalactic) is fixed to the best-fit parameters obtained for the overall time fit. While some variability may be present, limited statistics do not yet allow to make definite conclusions.

for variability, a  $\chi^2$  test was performed. The result for the light curve with 15 day bins is  $\chi^2/d.o.f. = 1.22$  and the probability is  $P(\chi^2) = 0.07$ . For the light curves with 30 day and 60 day bins we find  $\chi^2/d.o.f. = 1.37$  and  $\chi^2/d.o.f. = 1.32$ , corresponding to  $P(\chi^2) = 0.04$  and  $P(\chi^2) = 0.127$ , respectively. These results are consistent with no variability. Interestingly however, a similar test for the light curve with 45 day bins gives in  $\chi^2/d.o.f. \approx 1.61$  and  $P(\chi^2) = 0.015$ , indicating a possible variability on 45-day time scale. Unfortunately, because of limited statistics, we cannot make a definite conclusion in this regard. The light curve with 45 day bins is shown in Figure 4.2, with the dot-dashed line indicating the flux from the source for the whole time period (result of likelihood analysis).

In addition, the variability of observed flux above and below 4 GeV is performed. Low detection significance of the component above 4 GeV (TS=124.4) does not allow us to investigate possible variability timescale, whereas for the other component search of variability is performed for 15, 30, 45 and 60 day bins under the same screening conditions described above. So significant variability have been found in any time scale, however still the hints for the variability are present in the lightcurve of 45 day bins  $\chi^2/d.o.f. = 1.75$ .

## 4.4 Discussion and Conclusion-1

In the case of high-frequency-peaked BL Lac objects, homogeneous leptonic synchrotron-self-Compton (SSC) jet models often provide reasonable descriptions of their overall spectral energy distributions (SEDs). For Cen A, how-

ever, classical one-zone SSC models (under the proviso of modest Doppler beaming) are unable to satisfactorily account for its core SED up to the highest energies (cf. Chiaberge et al., 2001; Lenain et al., 2008; Abdo et al., 2010b). It seems thus well possible, that an additional component contributes to the observed emission at these energies (e.g., Lenain et al., 2008; Rieger and Aharonian, 2009). The results presented here indeed provides support for such a consideration. Our analysis of the 4 yr-data set reveals that the HE core spectrum

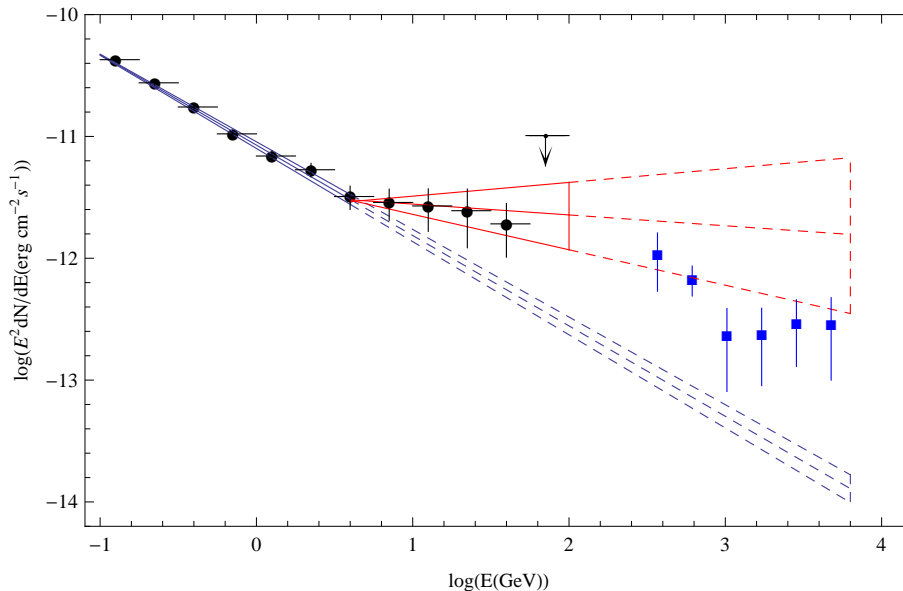


**Figure 4.3:** Gamma-ray spectrum for the core of Cen A from high (*Fermi*-LAT, this work) to very high (H.E.S.S., blue squares) energies. The blue bowtie represents a power-law with photon index 2.74, and the red bowtie a power-law with photon index 2.09. The dashed lines show extrapolations of these models to higher energies. The power-law extrapolation of the low-energy component (blue lines) would under-predict the fluxes observed at TeV energies.

of Cen A shows a “break” with photon index changing from  $\simeq 2.7$  to  $\simeq 2.1$  at an energy of  $E_b \simeq 4$  GeV. This break is unusual in that the spectrum gets harder instead of softer, while typically the opposite occurs. For a distance of 3.8 Mpc, the detected photon flux  $F_\gamma = (1.68 \pm 0.04) \times 10^{-7}$  photon  $\text{cm}^{-2}\text{s}^{-1}$  for the component below 4 GeV corresponds to an apparent (isotropic)  $\gamma$ -ray luminosity of  $L_\gamma(0.1 - 4 \text{ GeV}) \simeq 10^{41}$  erg  $\text{s}^{-1}$ . The component above 4 GeV, on the other hand, is characterized by an isotropic HE luminosity of  $L_\gamma(> 4\text{GeV}) \simeq 1.4 \times 10^{40}$  erg  $\text{s}^{-1}$ . This is an order of magnitude less when compared with the first component, but still larger than the VHE luminosity reported by H.E.S.S.  $L_\gamma(> 250 \text{ GeV}) = 2.6 \times 10^{39}$  erg  $\text{s}^{-1}$  Aharonian et al. (2009). All luminosities are below the Eddington luminosity corresponding to the black hole mass in Cen A; nevertheless, they are still quite impressive

when compared with the other nearby radio galaxy M87 containing a much more massive black hole.

Figure 4.3 shows the gamma-ray spectrum for the core of Cen A up to TeV energies. As one can see, the flux expected based on a power-law extrapolation of the low-energy component (below the break) clearly falls below the TeV flux reported by H.E.S.S.. Although the uncertainties in the photon index are large, it is clear that the spectrum becomes harder above 4 GeV. Remarkably, a simple extrapolation of the second (above the break) high-energy component to TeV energies could potentially allow one to match the average H.E.S.S. spectrum. These spectral considerations support the conclusion that we may actually be dealing with two (or perhaps even more) components contributing to the HE gamma-ray core spectrum of Cen A. Our analysis of the HE light curves provides some weak indication for a possible variability on 45 day time scale, but the statistics are not sufficient to draw clear inferences.

The limited angular resolution ( $\sim 5$  kpc) and the lack of significant variability introduces substantial uncertainties as to the production site of the HE gamma-ray emission. In principle, the hard HE component could originate from both a very compact (sub-pc) and/or extended (multi-kpc) region(s). The double-peaked nuclear SED of Cen A has been reasonably well-modeled up to a few GeV in terms of SSC processes occurring in its inner jet (e.g., Chiaberge et al., 2001; Abdo et al., 2010b). In this context, the hardening on the HE spectrum above 4 GeV would indeed mark the appearance of a physically different component. This additional component could in principle be related to a number of different (not mutually exclusive) scenarios, such as (i) non-thermal processes in its black hole magnetosphere Rieger and Aharonian (2009), (ii) multiple SSC-emitting components (i.e., differential beaming) Lenain et al. (2008) or (iii) photo-meson interactions of protons in the inner jet Kachelrieß et al. (2010); Sahu et al. (2012), (iv)  $\gamma$ -ray induced pair-cascades in a torus-like region (at  $\sim 10^3 r_s$ ) (e.g. Roustazadeh and Böttcher, 2011) (v) secondary Compton up-scattering of host galaxy starlight Stawarz et al. (2006) or (vi) inverse-Compton (IC) processes in the kpc-scale jet (e.g. Hardcastle and Croston, 2011). What concerns the more compact scenarios (i)-(iv) just mentioned: Opacity considerations do not a priori exclude a near-BH-origin, but could potentially affect the spectrum towards highest energies (e.g. Rieger, 2011). A SSC multi-blob VHE contribution, on the other hand, requires the soft gamma-rays to be due to synchrotron instead of IC processes, in which case correlated variability might be expected. Photo-meson ( $p\gamma$ ) interactions with, e.g., UV or IR background photons ( $n_\gamma$ ) require the presence of UHECR protons, which seems feasible for Cen A. However, as the mean free paths  $\lambda \sim 1/(\sigma_{p\gamma} n_\gamma K_p)$  of protons through the relevant photon fields are comparatively large, usually only a modest fraction of the proton energy can be converted into secondary particles. Models of this type thus tend to need an injection power in high-energy protons exceeding the average jet power of  $\sim 10^{43-44}$

erg/s (e.g. Yang et al., 2012). The efficiency of IC-supported pair cascades in Cen A, on the other hand, appears constrained by low accretion modes and the possible absence of a dust torus. Considering the more extended scenarios (v)-(vi): Partial absorption ( $\sim 1\%$ ) of nuclear gamma-rays by starlight in the inner part of the host galaxy, and subsequent up-scattering of starlight photons could potentially introduce another HE contribution. However, the efficiency for this process is low, so that a high VHE injection power into the ambient medium is required, and the predicted spectral shape does not seem to match well. Compton-upscattering of starlight photon by energetic electrons in the kpc-scale jet also seems to have difficulties in reproducing the noted HE characteristics.

Finally, let us mention that gamma-ray production may perhaps also be related to relativistic protons interacting with the ambient gas in the large (kpc) scale regions, e.g., the overall elliptical galaxy NGC 5128 or the densest part of its dust lane. Note that the  $\gamma$ -ray luminosity  $\approx 10^{41}$  erg/s above 100 MeV is larger by two orders of magnitude than the  $\gamma$ -ray luminosity of the Milky Way, which could be related to a higher rate of cosmic-ray production and a more effective confinement in the case of NGC 5128. Moreover, gamma-rays might also be produced in a diluted  $R_{\text{halo}} \sim 30$  kpc (halo) region of this galaxy. Despite the low density of gas, gamma-ray production on characteristic timescale  $t_{\text{pp}} \approx 3 \times 10^9 (n/10^{-2} \text{cm}^{-3})^{-1}$  yr can be effective, even for a relatively fast diffusion of cosmic rays in this region. More specifically, the efficiency could be close to one, if the diffusion coefficient at multi-GeV energies does not exceed  $D \sim R_{\text{halo}}^2/t_{\text{pp}} \sim 10^{29} \text{cm}^2/\text{s}$ . This seems an interesting possibility, especially for the second (hard) HE component with photon index close to 2.1, in the context of its similarity to the gamma-ray spectrum of the so-called 'Fermi Bubbles' around the center of our Galaxy Su et al. (2010). The much higher luminosity (by  $\sim 2 - 3$  orders of magnitude) of the second component compared to the gamma-ray luminosity of the Fermi Bubbles seems quite natural, given the much larger energy available in Cen A, in particular in the form of kinetic energy of its jet.

The results presented here provide observational evidence for an additional contribution at the highest energies and a more complex spectral gamma-ray behavior than previously anticipated. While considerations like those mentioned above may lead one to favor one production scenario over the other, none of them cannot be easily discarded. In fact, it is well conceivable that several of them contribute to the observed gamma-ray emission. Definite progress in this regard could be achieved in case of a significant detection of gamma-ray time variability.

## 4.5 The lobes of Cen A

The data used for the study of  $\gamma$ -ray emission from the lobes of CenA are from the beginning of the operation until November 14, 2011, amounting to  $\sim 3$  yr of data (MET 239557417– 342956687). We used the standard LAT analysis software (v9r23p1)<sup>2</sup>. To avoid systematic errors due to poor determination of the effective area at low energies, we selected only events with energies above 200 MeV. The region-of-interest (ROI) was selected to be a rectangular region of size  $14^\circ \times 14^\circ$  centered on the position of Cen A (RA =  $201^\circ 21' 54''$ , DEC =  $-43^\circ 1' 9''$ ). To reduce the effect of Earth albedo backgrounds, time intervals when the Earth was appreciably in the FoV (specifically, when the center of the FoV was more than  $52^\circ$  from zenith) as well as time intervals when parts of the ROI were observed at zenith angles  $> 105^\circ$  were also excluded from the analysis. The spectral analysis was performed based on the P7v6 version of the post-launch instrument response functions (IRFs). We modeled the Galactic background component using the LAT standard diffuse background model *gal\_2yearp7v6\_v0* and we left the overall normalization and index as free parameters. We also used *iso\_p7v6source* as the isotropic  $\gamma$ -ray background.

The resulting Fermi-LAT counts map for the 3 yr data set is shown in Figure 4.4(a). The (green) crosses show the position of the point-like sources from the 2FGL catalog (Nolan et al. (2012)) within the ROI. Extended emission to the north and south of Cen A is detected with significances of  $TS > 100$  ( $10 \sigma$ ) and  $TS > 400$  ( $20 \sigma$ ), respectively.

### 4.5.1 Spatial analysis

Events with energies between 200 MeV and 30 GeV were selected. The residual image after subtracting the diffuse background and point-like sources including the core of Cen A is shown in Figure 4.4(b). The fluxes and spectral indices of 11 other point-like sources generated from the 2FGL catalog within the ROI are also left as free parameters in the analysis. The 2FGL catalog source positions are shown in Figure 4.4(a), where 2FGL J1324.0-4330e accounts for the lobes (both north and south). A new point-like source (2FGL J1335.3-4058), located at RA =  $203^\circ 49' 30''$ , DEC =  $-40^\circ 34' 48''$  accounts for some residual emission from the north lobe, although no known source at other wavelengths is found to be associated. We treat it as part of the north lobe here. The core of Cen A is modeled as a point-like source. Then the following steps were performed:

(1) To evaluate the total (extended) HE  $\gamma$ -ray emission we first used a template based on the residual map (T1; corresponding to the blue contours in

---

<sup>2</sup><http://fermi.gsfc.nasa.gov/ssc>

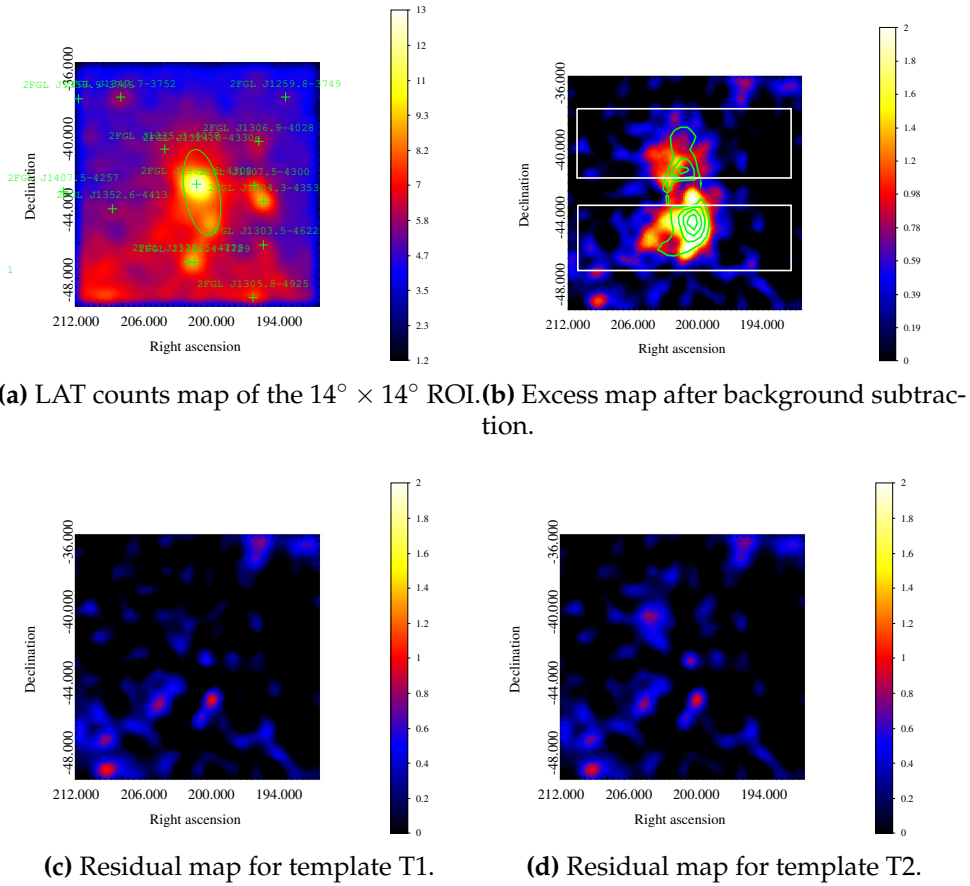


**Figure 4.4:** The different maps for the Cen A region: (a) LAT counts map of the  $14^\circ \times 14^\circ$  region of interest (ROI) around the position of Cen A. The counts map is smoothed with a Gaussian of kernel  $0.8^\circ$ . The green crosses mark the position of the 2FGL point-like sources. (b) Excess map after subtraction of diffuse background, point-like sources and Cen A core. The contours are WMAP radio lobe contours, while the white boxes represent the projection regions discussed in Sec. 4.5.1. (c) Residual map using template T1 for the lobes. (d) Residual map using the radio template T2 for the lobes.

Figure 4.5). The TS values for the south and the north lobe in this template are 411 and 155, respectively. The residual map was also compared with radio (WMAP, 22 GHz) lobe contours (green contours overlaid on Figure 4.4(b)). While lower-frequency radio maps exist, we expect the higher-frequency 22 GHz map to better represent the GeV-emitting particles. We find that the south lobe of the HE  $\gamma$ -ray image is similar to the south lobe of the radio one, whereas the HE emission in the north extends beyond the radio lobe emission region.

(2) To understand this feature better, we re-fitted the excess using an additional template (T2; red contours in Figure 4.6) generated from the radio (WMAP) image. The two templates are shown in Figure 4.5, and the corresponding residual maps are shown in Figure 4.4. While there is some residual emission to the north of Cen A for template T2, this residual emission is obviously absent from template T1. The qualitative features of the different residual maps are confirmed by the corresponding TS values, which are listed in Table 4.1. Accordingly, the HE south lobe seems to agree reasonably well with the radio south lobe, whereas for the north lobe, the template generated from the radio lobe (T2) fits the HE excess substantially worse than T1 (110 vs 155).

**Table 4.1:** TS value for the two templates used.

Model	north Lobe	south Lobe
T1	155	411
T2	110	406

(3) To further investigate a possible extension (or contribution of a background source) of the north lobe, we evaluated the projection of a rectangular region on the excess image (in white in Figure 4.4(b)). Figure 4.6 shows the projection for the north and south regions for Fermi-LAT image (in black) and the radio one (in red). The south projection for the radio map is well-fitted by a single Gaussian centered at  $\sim 0.05$  (0 is defined as the center of the rectangle on  $RA = 201^{\circ}21'54''$ ,  $DEC = -43^{\circ}1'9''$ ) with an extension of  $\sigma = 0.99^{\circ}$ . For the Fermi-LAT map the Gaussian is centered at  $\sim 0.5$  and has  $\sigma = 1.01^{\circ}$ , compatible with the radio map projection. In contrast, the north projection for the Fermi-LAT map has a Gaussian profile with  $\sigma = 1.68^{\circ}$ , while for the radio map  $\sigma$  is  $0.97^{\circ}$ . The extension in the north projections for the Fermi-LAT map indicates that the  $\gamma$ -ray north lobe is more extended than the radio one or that an (otherwise unknown) source in the background may be contributing to the total emission.

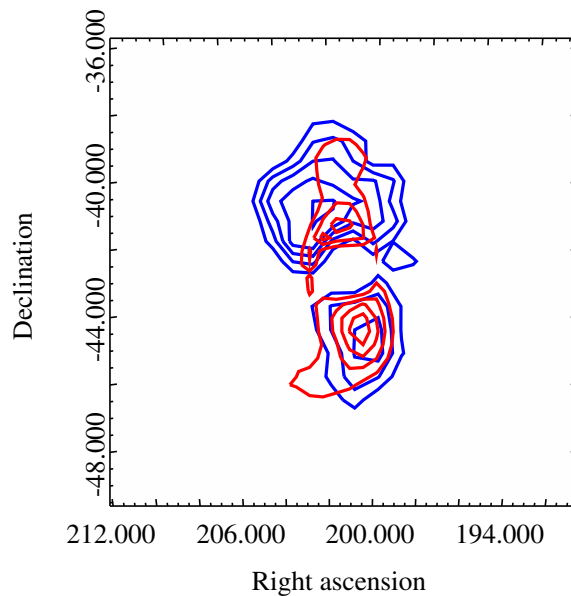


**Figure 4.5:** Two templates used in the analysis. The blue contours correspond to T1 and the red to T2.

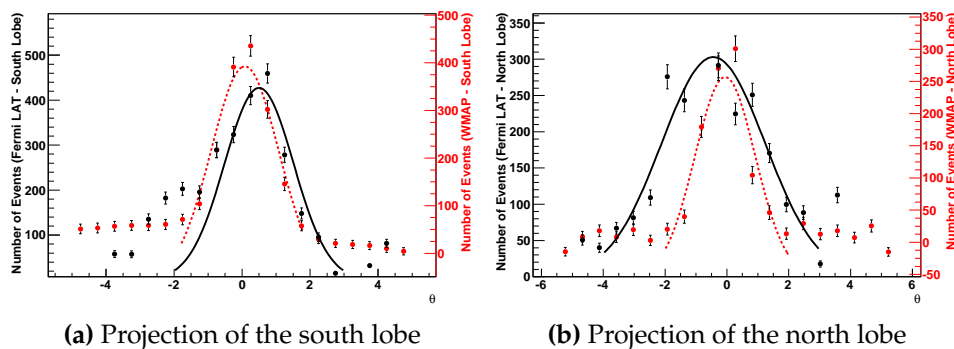


**Figure 4.6:** Projection of the rectangular region shown in Figure 4.4(b) for both lobes. The curves are Gaussian fits, with WMAP data in red and Fermi-LAT data in black. Units for the positional (x) axis are degrees.

### 4.5.2 Spectral analysis

Our morphological analysis indicates some incongruity between the morphology of the radio lobe and  $\gamma$ -ray lobe in the north. Hence, to model the  $\gamma$ -ray lobe as self-consistently as possible, we used the template generated with the residual map (T1). Integrating the whole  $\gamma$ -ray emission observed, we then derived the total flux and index in the 100 MeV to 30 GeV energy range.

For the north lobe the integral HE flux is  $(0.93 \pm 0.09) \times 10^{-7} \text{ph cm}^{-2}\text{s}^{-1}$  and the photon index is  $2.24 \pm 0.08$ , while for the south lobe we find  $(1.4 \pm 0.2) \times 10^{-7} \text{ph cm}^{-2}\text{s}^{-1}$  and  $2.57 \pm 0.07$ , respectively. The results are summarized in Table 4.2, where the subscripts 3a and 10m refer to the three-year data (analyzed here) and the ten-month data (reported in Abdo et al. (2010a)), respectively. We find that the flux and photon indices in the T2 templates are similar to the ten-month data. On the other hand, the analysis using the T1 template results in a harder spectrum for the north lobe.

To derive the spectral energy distribution (SED) we divided the energy range into logarithmically spaced bands and applied *gtlike* in each of these bands. Only the energy bins for which a signal was detected with a significance of at least  $2\sigma$  were considered, while an upper limit was calculated for those below. As a result, there are seven bins in the SED for the south lobe.

To clarify the origin of the  $\gamma$ -ray emission, we evaluated the spectrum in different parts of each lobe. To this end, we divided each lobe into two parts and used *gtlike* to evaluate the spectrum. In the south lobe the resulting photon index is  $2.8 \pm 0.2$  near the Cen A core and  $2.3 \pm 0.1$  far away from the core. Unfortunately, the statistics are still not high enough to claim a clear hardening of the spectrum. For the northern lobe, both parts appear to be consistent with values of  $2.2 \pm 0.2$ .

**Table 4.2:** Fluxes and spectra of the lobes

Source Name	$\Phi_{3a}(\text{T1})$	$\Gamma_{3a}(\text{T1})$	$\Phi_{10m}$	$\Gamma_{10m}$	$\Phi_{3a}(\text{T2})$	$\Gamma_{3a}(\text{T2})$
South Lobe	$1.43 \pm 0.15$	$2.57 \pm 0.07$	$1.09 \pm 0.24$	$2.60 \pm 0.15$	$1.40 \pm 0.15$	$2.56 \pm 0.08$
North Lobe	$0.93 \pm 0.09$	$2.24 \pm 0.08$	$0.77 \pm 0.20$	$2.52 \pm 0.16$	$0.64 \pm 0.15$	$2.56 \pm 0.08$

$\Phi$  is the integral flux (100 MeV to 30 GeV) in units of  $10^{-7} \text{ph} \cdot \text{cm}^{-2}\text{s}^{-1}$  and  $\Gamma$  is the photon index. The subscripts "3a" and "10m" refer to the three-year data analyzed here and to the ten-month results (based on a WMAP template) reported in Abdo et al. (2010a), respectively.

## 4.6 The origin of the non-thermal lobe emission

Using the WMAP and Fermi-LAT results reported here, we can characterize the spectral energy distributions for the north and the south lobe. While the radio emission is usually taken to be caused by electron synchrotron emission, the origin of the HE  $\gamma$ -ray emission could in principle be related to both leptonic (inverse-Compton scattering) and hadronic (e.g., pp-interaction) processes. In the following we discuss possible constraints for the underlying radiation mechanism as imposed by the observed SEDs.

### 4.6.1 Inverse-Compton origin of $\gamma$ -rays

Both the HE  $\gamma$ -ray and the radio emission could be accounted for in a leptonic scenario. In the simplest version, a single population of electrons  $N(\gamma, t)$  is used to model the SED through synchrotron and inverse-Compton emission, with particle acceleration being implicitly treated by an effective injection term  $Q = Q(\gamma, t)$ . The latter allows us to distinguish acceleration caused by, e.g., multiple shocks or stochastic processes (e.g., O’Sullivan et al. (2009)) from emission, and enables a straightforward interpretation. The kinetic equation describing the energetic and temporal evolution of the radiating electrons can then be written as

$$\frac{\partial N}{\partial t} = \frac{\partial}{\partial \gamma} (P N) - \frac{N}{\tau_{\text{esc}}} + Q, \quad (4.6.1)$$

where  $P = P(\gamma) = -\frac{d\gamma}{dt}$  is the (time-independent) energy loss rate and  $\tau_{\text{esc}}$  is the characteristic escape time. For negligible escape (as appropriate here, given the large size of the  $\gamma$ -ray emitting region) and quasi continuous injection (considered as a suitable first-order approximation given the short lifetime of TeV electrons and the scales of the lobes)  $Q(\gamma, t) = Q(\gamma)$ , the solution of the kinetic equation becomes

$$N(\gamma, t) = \frac{1}{P(\gamma)} \int_{\gamma}^{\gamma_0} Q(\gamma) d\gamma, \quad (4.6.2)$$

where  $\gamma_0$  is found by solving the characteristic equation for a given epoch  $t$ ,  $t = \int_{\gamma}^{\gamma_0} \frac{d\gamma}{P(\gamma)}$  (e.g., Atoyan and Aharonian (1999)). If synchrotron or inverse-Compton (Thomson) losses ( $P(\gamma) = a \gamma^2$ ) provide the dominant loss channel, then  $\gamma_0 = \gamma / (1 - a\gamma t)$ , so that at the energy  $\gamma_{\text{br}} = \frac{1}{a t}$  the stationary power-law electron injection spectrum steepens by a factor of 1 (cooling break) due to radiative losses, naturally generating a broken power-law.

We used the above particle distribution described in eq. (4.6.2) for a representation of the observed lobe SEDs. The magnetic field strength  $B$ , the maximum electron energy  $\gamma_{\text{max}}$  and the epoch time  $t$  were left as free parameters to model the data. Klein-Nishina (KN) effects on the inverse-Compton-scattered HE spectrum were taken into account (following Aharonian and Atoyan (1981)). Figure 4.7 shows the SED results obtained for the north and south lobes. The HE part of both spectra can be described by a power-law with photon index  $\Gamma_{\gamma} \simeq 2.2$  and  $2.6$  for the north and the south lobe, respectively. At low energies, the south lobe spectrum shows a synchrotron peak at about 5 GHz, while the north lobe is well described by a power-law with an index  $> 2$ . Note that if one would use a simple power-law electron injection spectrum  $Q(\gamma) \propto \gamma^{-\alpha}$ , evolving in time with a cooling break, to describe the HE  $\gamma$ -ray spectrum, a power index  $\alpha = 3.2$  would be required for the south lobe.

Yet, assuming that the same electron population is responsible for both the radio-synchrotron and HE inverse-Compton emission, such a value would be in conflict with the results obtained from the WMAP data analysis, indicating an electron population with power-law index  $\alpha \simeq 2$  based on the detected synchrotron emission. As it turns out, however, this problem could be accommodated by considering a more natural spectral input shape, e.g., an electron injection spectrum with an exponential cut-off

$$Q(\gamma) = Q_0 \gamma^{-\alpha} \exp\left(-\frac{\gamma}{\gamma_{\max}}\right), \quad (4.6.3)$$

where the constant  $Q_0$  can be obtained from the normalization to the injection power  $L = m_e c^2 \int Q(\gamma) \gamma d\gamma$ .

The age of the giant lobe emission, and associated with this, the duration of particle acceleration activity, is somewhat uncertain. Dynamical arguments suggest a lower limit  $> 10^7$  yr for the giant radio lobes, while synchrotron spectral aging arguments indicate an age  $\lesssim 3 \times 10^7$  yr (e.g., Israel (1998); Alvarez et al. (2000); Hardcastle et al. (2009)). The observed GeV extension in itself would already imply an extreme lower limit of  $R/c > 10^6$  yr. In the following we therefore discuss the SED implications for an epoch time  $t$  between  $10^7$  yr and  $10^8$  yr. As it turns out, the modeling of the GeV data provides support for a maximum lobe age of  $\sim 8 \times 10^7$  yr.

For the south lobe, the radio data suggest a break frequency  $\nu_{\text{br}} = 5$  GHz above which the spectrum drops abruptly. The break in the synchrotron spectrum is related to the break in the electron spectrum via  $\nu_{\text{br}} = 1.3 \gamma_{\text{br}}^2 B_{1\mu\text{G}}$  Hz. In principle, a change in the spectral shape of the electron population might be caused by cooling effects or/and the existence of a maximum energy for the electron population. For a minimum epoch time  $t_{\text{min}} = 10^7$  yr, cooling would affect the synchrotron spectrum at frequency  $\approx 80 B_{1\mu\text{G}}$  GHz, much higher than inferred from the radio data. Therefore, to obtain a break at 5 GHz in the south lobe, a maximum energy in the electron population ( $\gamma_{\max}$ ), lower than  $\gamma_{\text{br}}$  defined by  $t = t_{\text{min}}$  would be needed. On the other hand, for a maximum epoch time  $t_{\text{max}} = 8 \times 10^7$  yr, the power-law spectral index changes at frequency  $\simeq 1 B_{1\mu\text{G}}$  GHz, providing a satisfactory agreement with the radio data. In this case the maximum electron energy is obtained from the radio data above the break frequency 5 GHz. Results for the considered minimum and maximum epoch time, and for a fixed power-law electron index  $\alpha = 2$  are illustrated in Figures 4.7 and 4.8. Note that for  $B \leq 3\mu\text{G}$ , the energy loss rate  $P(\gamma)$  is dominated by the IC channel only, so that the results of the calculations are quite robust.

Figure 4.7 shows a representation of the SED for the north and the south lobe, respectively, using the parameters  $t_{\text{min}} = 10^7$  yr and  $\gamma_{\max} = 1.5 \times 10^5$ . The dashed line shows the HE contribution produced by inverse-Compton scattering of cosmic microwave background photons by relativistic electrons

within the lobes. In this case the resulting  $\gamma$ -ray flux can only describe the first two data points and then drops rapidly. Consequently, to be able to account for the observed HE spectrum, extragalactic background light photons need to be included in addition to CMB photons (see dot-dashed line in Figure 4.7). Upscattering of infrared-to-optical EBL photons was already required in the stationary leptonic model reported in the original Fermi paper (Abdo et al. (2010a)). In our approach we adopt the model by Franceschini et al. (2008) to evaluate this EBL contribution. The solid line in Figure 4.7 represents the total (CMB+EBL) inverse-Compton contribution. The maximum total energy of electrons in both lobes is found to be  $\sim 2 \times 10^{58}$  erg and the energy in the magnetic fields is roughly 25% of this. Dividing the total energy by the epoch time  $10^7$  yr would imply a mean kinetic power of the jets inflating the lobes of  $\simeq 7 \times 10^{43}$  erg/s, roughly two orders of magnitude lower than the Eddington power inferred for the black hole mass in Cen A, yet somewhat above the estimated power of the kpc-scale jet in the current epoch of jet activity (Croston et al. (2009)). This could indicate that the jet was more powerful in the past. Obviously, the requirement on the mean jet power can be significantly reduced if one assumes an older age of the lobes.

Figure 4.8 shows a representation of the SED for an epoch time  $t_{\max} = 8 \times 10^7$  yr, with a maximum electron Lorentz factor  $\gamma_{\max} = 2.5 \times 10^6$  and  $1.5 \times 10^6$  for the north lobe and the south lobe, respectively. Note that in this case the contribution by inverse-Compton scattering of CMB photons alone is sufficient to account for the observed HE spectrum (see the solid line in Figure 4.8). The inverse-Compton contribution of EBL photons only becomes important at higher energies (see the dot-dashed line in Figure 4.8). On the other hand, for an epoch time  $t$  exceeding  $t_{\max} = 8 \times 10^7$  yr, the high-energy part of the SED would no longer be consistent with the data (see the dashed line in Figure 4.8 for  $t = 10^8$  yr). This could be interpreted as additional evidence for a finite age  $< 10^8$  yr of the lobes. The maximum total energy of electrons in both lobes is found to be  $\approx 6 \times 10^{57}$  erg, with the total energy in particles and fields comparable to the  $10^7$ yr-case, thus requiring only a relatively modest mean kinetic jet power of  $\sim 10^{43}$  erg/s.

### 4.6.2 Hadronic $\gamma$ -rays?

Once protons are efficiently injected, they are likely to remain energetic since the cooling time for pp-interactions is  $t_{pp} \approx 10^{15}(n/1 \text{ cm}^{-3})^{-1}$  s. High-energy protons interacting with the ambient low-density plasma can then produce daughter mesons and the  $\pi^0$  component decays into two  $\gamma$ -rays. The data reported here allow us to derive an upper limit on the energetic protons contained in the lobes of Cen A. As before, we use a power-law proton distri-

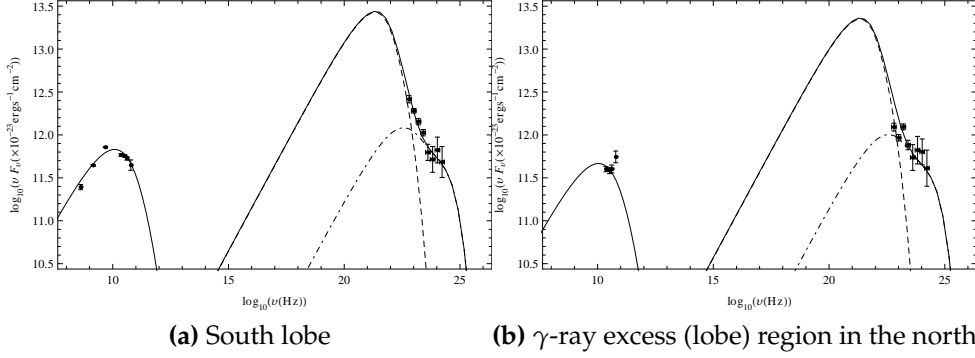


**Figure 4.7:** Synchrotron and inverse-Compton fluxes for  $t = 10^7$  yr. The radio data for the south lobe are from Hardcastle et al. (2009) (sum of region 4 and region 5 in their Table 1), while the radio data for the north region are from the WMAP analysis in this paper. The mean magnetic field value  $B$  used for the north and the south lobe is  $0.39 \mu\text{G}$  and  $0.43 \mu\text{G}$ , respectively. The dot-dashed line refers to the IC contribution due to EBL upscattering.

bution with an exponential cut-off, i.e.,

$$N(\gamma_p) = N_0 \gamma_p^{-\alpha} \exp\left(-\frac{\gamma_p}{\gamma_{\max}}\right)$$

where the constant  $N_0$  can be expressed in terms of the total proton energy  $W_p = m_p c^2 \int \gamma_p N(\gamma_p) d\gamma_p$ . Current estimates for the thermal plasma density in the giant radio lobes of Cen A suggest a value in the range  $n \simeq (10^{-5} - 10^{-4}) \text{ cm}^{-3}$  (e.g., Isobe et al. (2001); Feain et al. (2009)). We used  $n = 10^{-4} \text{ cm}^{-3}$  for the model representation shown in dotted line in Figure 4.8. In both lobes, the power-law index of the proton population is  $\alpha = 2.1$ , and the high-energy cut-off is  $E_{\max} \simeq 55 \text{ GeV}$ . The maximum total energy  $W_p$  is proportional to the gas number density  $n$ , so that  $W_p \simeq 10^{61} (n/10^{-4} \text{ cm}^{-3})^{-1} \text{ erg}$ , obtained here, should be considered as an upper limit. In principle, protons could be accumulated over the whole evolutionary timescale of the lobes. For a long timescale of  $\geq 10^9$  yr, an average injection power  $\leq 3 \times 10^{44} \text{ erg/s}$  and a mean cosmic-ray diffusion coefficient of  $D \sim R^2/t \lesssim 3 \times 10^{30} (R/100 \text{ kpc})^2 \text{ cm}^2/\text{s}$  would be needed.

## 4.7 Discussion and conclusion-2

Results based on an detailed analysis of 3 yr of Fermi-LAT data on the giant radio lobes of Cen A shows that they are detected with a significance more than twice as high as reported before (i.e., with more than  $10$  and  $20\sigma$  for the northern and the southern lobe, respectively) which allows a better

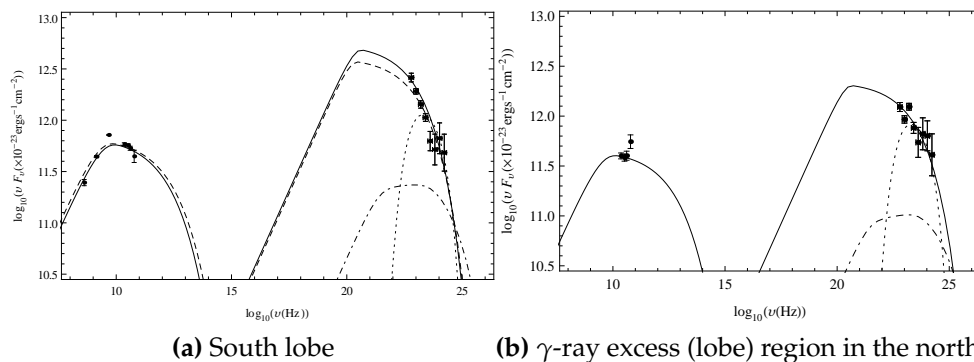


**Figure 4.8:** Synchrotron and inverse-Compton fluxes for  $t = 8 \times 10^7$  yr. The mean magnetic field value  $B$  for the south lobe and the  $\gamma$ -ray excess region in the north lobe is  $0.91 \mu\text{G}$  and  $1.17 \mu\text{G}$ , respectively. The dot-dashed line refers to the IC contribution due to EBL upscattering. The dashed line (a) shows the result for  $t = 10^8$  yr. The possible  $\gamma$ -ray flux expected from pp-interactions for a thermal gas density  $n = 10^{-4} \text{ cm}^{-3}$  are also shown (dotted line).

determination of their spectral features and morphology. A comparison of the Fermi-LAT data with WMAP data indicates that the HE  $\gamma$ -ray emission regions do not fully coincide with the radio lobes. There is of course no a priori reason for them to coincide. The results reported here particularly support a substantial HE  $\gamma$ -ray extension beyond the WMAP radio image for the northern lobe of Cen A. We have reconstructed the SED based on data from the same emission region. A satisfactory representation is possible in a time-dependent leptonic scenario with radiative cooling taken into account self-consistently and injection described by a single power-law with exponential cut-off. The results imply a finite age  $< 10^8$  yr of the lobes and a mean magnetic field strength  $B \lesssim 1 \mu\text{G}$ . While for lobe lifetimes on the order of  $8 \times 10^7$  yr, inverse-Compton up-scattering of CMB photons alone would be sufficient to account for the observed HE spectrum, up-scattering of EBL photons is needed for shorter lobe lifetimes. In a leptonic framework, the HE emission directly traces (via inverse-Compton scattering) the underlying relativistic electron distribution and thereby provides a spatial diagnostic tool. The radio emission, arising from synchrotron radiation, on the other hand also traces the magnetic field distribution. Together, the HE  $\gamma$ -ray and the radio emission thus offer important insights into the physical conditions of the source. That the HE emission seems extended beyond the radio image could then be interpreted as caused by a change in the magnetic field characterizing the region. This would imply that our quasi-homogeneous SED model for the HE lobes can only serve as a first-order approximation and that more detailed scenarios need to be constructed to fully describe the data. This also applies to the need of incorporating electron re-acceleration self-consistently.

Extended HE emission could in principle also be related to a contribution from hadronic processes. The cooling timescales for protons appear much more favorable. On the other hand, both the spectral shape of the lobes and the required energetics seem to disfavor pp-interaction processes as sole contributor.

# 5 On the Detectability of High-Energy Galactic Neutrino Sources

## 5.1 Introduction

The search for neutrinos with  $E_\nu > \text{TeV}$  Lipari (2006) with telescopes of volumes in the  $\text{km}^3$  scale is considered important. IceCube is collecting exposures of the order of  $\text{km}^2 \times \text{year}$  and this will be continued and extended by KM3NeT.<sup>1</sup> As has happened in the past (e.g., for X-ray searches) the new instruments could eventually lead to surprising outcomes. The hope for surprises is certainly one strong motivation of the search for the sources of high energy neutrinos that plausibly are also sources of cosmic rays. At the same time, there are many reasons why we would like to have defined expectations on high energy neutrinos: to interpret the results of the observations, to plan the future research, to better focus our goals, to optimize the new instruments. The trouble is that the hypotheses on which the present expectations are based are still rather uncertain and difficult to test. Thus we do not have reliable predictions yet, and this limits our capability to plan the next steps.

Here we focus on this aspect of the search for high energy neutrino sources that we are now beginning. We discuss several aspects: We emphasize the relevance of  $\gamma$ -ray observations in the 10-100 TeV energy range for high energy neutrinos; we analyze the prospect to understand better certain  $\gamma$ -ray sources that have a special theoretical interest in connection with high energy neutrinos; we clarify the argument in favor of a neutrino telescope in the Northern hemisphere. We focus on the subclass of galactic sources that are of particular interest for future instruments located in the Northern hemisphere.

The outline of this chapter is as follows. First, considering the high energy  $\gamma$ -ray sources that are transparent to the radiation, we characterize those of them that could be, at the same time, bright enough neutrino sources (Sec. 5.2). Next, after recalling the relevant theoretical context, we discuss the prospects of obtaining more defined expectations for one of the most interesting of these  $\gamma$ -ray sources, namely, the young supernova remnant named

---

<sup>1</sup>All considerations below apply to any large (i.e., with volumes of the order of one  $\text{km}^3$ ) neutrino telescope of the Northern hemisphere; KM3NeT is taken as an example, being the most advanced project of this type at present.

$N_\gamma$	$E_c =$						
	$10^0$	$10^{0.5}$	$10^1$	$10^{1.5}$	$10^2$	$10^{2.5}$	$10^3$
$\alpha = 1.8$	70	16	4.9	2.1	1.1	0.7	0.5
1.9	86	20	6.7	3.0	1.7	1.1	0.8
2.0	110	25	9.0	4.2	2.5	1.7	1.3
2.1	130	32	12	5.9	3.5	2.5	2.0
2.2	160	41	16	8.0	5.0	3.6	3.0

**Table 5.1:** Normalization of the  $\gamma$ -ray fluxes  $N_\gamma$ , in units of  $10^{-12}/(\text{cm}^2 \text{ s TeV})$  that corresponds to an induced flux  $I_{\mu+\bar{\mu}}(> 1\text{TeV}) = 1/(\text{km}^2\text{yr})$ . First column: slope of the  $\gamma$ -ray flux,  $\alpha$ . First row: cutoff energy of the  $\gamma$ -ray spectrum,  $E_c$ , measured in TeV. See Eq. 5.2.1.

RX J1713.7-3946 (Sec. 5.3). Finally, we quantify in Sec. 5.4 the importance of monitoring the Southern high energy neutrino sky on the basis of the Galactic matter distribution.

## 5.2 Using high energy $\gamma$ -rays as a guide for high energy neutrino search

Here we consider a precise assumption on the astrophysical neutrino sources: We suppose that they are transparent to the very high energy gamma radiation. In this way we can derive upper limits on neutrinos, by postulating that *all*  $\gamma$ -rays originate from proton-proton collisions. In fact, the yield of neutral mesons and of charged mesons are strictly connected and there is a linear relation between the fluxes of high energy  $\gamma$ -rays and neutrinos (Vissani (2006), Villante and Vissani (2008)).

We can then quantify the concept of “promising”  $\gamma$ -ray sources. Suppose that the  $\gamma$ -ray flux has the form:

$$I_\gamma(E_\gamma) = N_\gamma \times (E_\gamma/1 \text{ TeV})^{-\alpha} \times \exp \left[ -\sqrt{E_\gamma/E_c} \right], \quad (5.2.1)$$

where we consider the ranges of parameters:  $\alpha = 1.8 - 2.2$  (=slope) and  $E_c = 1 \text{ TeV} - 1 \text{ PeV}$  (=energy cutoff). This form corresponds to an exponential cutoff in the spectrum of the cosmic rays that generate the  $\gamma$ -rays, see Kappes et al. (2007), and has been tested for adequacy on the available  $\gamma$ -ray data. Following Villante and Vissani (2008), and requiring an induced flux of 1 muon or antimuon per  $\text{km}^2$  per year above 1 TeV (i.e. 1 signal event in a conventional neutrino telescope with an exposure of  $1 \text{ km}^2 \times \text{yr}$ ), we determine  $N_\gamma$  for each value of  $\alpha$  and  $E_c$ ; the results are given in Tab. 5.1 and are further illustrated in Figure 5.1. This table and this figure identify the

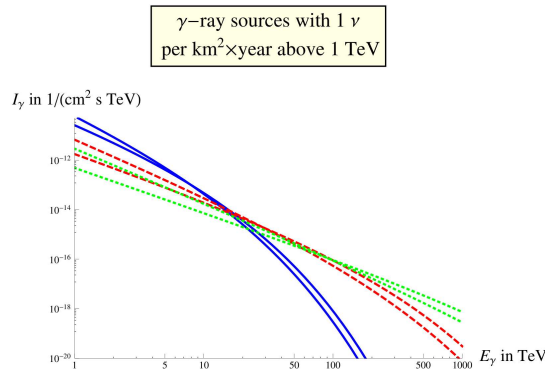


**Figure 5.1:** Fluxes of  $\gamma$ -rays corresponding to 1 event above 1 TeV in a neutrino telescope with an exposure of  $1 \text{ km}^2 \times \text{yr}$ , as given in Eq. 5.2.1 and Tab. 5.1. We selected the values  $\alpha = 1.8$  and  $2.2$  (the first being smaller at low energies and larger at high energies) and  $E_c = 1, 10^{1.5}$  and  $10^3$  TeV (continuous, dashed and dotted lines, respectively).

transparent  $\gamma$ -ray sources that could be interesting neutrino sources. There is a wide variety of possibilities, ranging from intense  $\gamma$ -ray sources to weak ones; this is due to the fact that the main contribution to the neutrino signal is from energies larger than 1 TeV, where we still have limited information from  $\gamma$ -ray observations.

By a systematic exploration of the  $\gamma$ -ray sky till  $E_\gamma \sim 100$  TeV and of the sources with an intensity above  $10^{-12} / (\text{cm}^2 \text{ s TeV})$  at 1 TeV, we could have a guide for the search of very high energy neutrinos, at least for the sources that are transparent to their  $\gamma$ -ray radiation. It is interesting to note that at 20 TeV, all fluxes of Tab. 5.1 are in the narrow range

$$I_\gamma(20 \text{ TeV}) = (2 - 6) \times 10^{-15} \text{ ph}/ (\text{cm}^2 \text{ s TeV}) \quad (5.2.2)$$

that characterizes the region of energies and of intensities where the  $\gamma$ -ray observations are more relevant for the high energy neutrino detectors: see again Figure 5.1. We remark that Eq. 5.2.2 is a new result. Its relevance can be understood better by recalling that the existing  $\gamma$ -ray detectors have explored mostly the region of energy around the TeV. Thus, the future  $\gamma$ -ray measurements in the region 10-100 TeV—e.g. those by the Cherenkov Telescope Array (CTA) instrument—will have an important impact on the expectations of high energy neutrinos. In summary, it will be possible to clarify the expectations of neutrino astronomy, by the measurements of future  $\gamma$ -ray observatories.

**SNR as a major example of transparent  $\gamma$ -ray source** Shell type supernova remnants (SNR) are an important example of astronomical sources of  $\gamma$ -rays that is expected to be transparent to their  $\gamma$ -ray emission. A few young

SNR, recently observed in the TeV range,<sup>2</sup> are known to exceed the bound in Eq. 5.2.2, thus being of particular interest. We discuss them here to illustrate the issue further:

- The first example is the supernova remnant called RX J1713.7-3946 and measured by HESS, **Aharonian** et al. (2007b). It has a  $\gamma$ -ray spectrum that is reasonably well described assuming  $\alpha = 1.79 \pm 0.06$  and  $E_c = 3.7 \pm 1$  TeV in Eq. 5.2.1 (Villante and Vissani (2007)) and that has an intensity at 20 TeV of  $(1.7 \pm 0.3) \times 10^{-14}$  / (cm<sup>2</sup> s TeV). Correspondingly, the maximum value of the neutrino signal from this source is larger than 1 event per km<sup>2</sup> per year, and more precisely we have:

$$I_{\mu+\bar{\mu}}(> 1 \text{ TeV}) = (2.4 \pm 0.3 \pm 0.5) / (\text{km}^2 \text{ yr}) \quad (5.2.3)$$

see Tab. 2 and Sect. IV of Villante and Vissani (2008).

- A second example is the SNR called Vela Jr (RX J0852. 0-4622) as observed in **Aharonian** et al. (2007a). The available  $\gamma$ -ray observations of this object are less complete. Its measured spectrum has been described simply by a power law and its emission at 20 TeV is in the range  $(1 - 3) \times 10^{-14}$  / (cm<sup>2</sup> s TeV); however, 20 TeV is the highest measured energy.

Note that both these SNR's are in the South  $\gamma$ -ray sky, and are thus potentially interesting for neutrino telescopes located in the Northern hemisphere (see Sec. 5.4). In the next section, we recall the reasons why such SNR's are considered interesting and discuss in more details the present understanding of RX J1713.7-3946 and the prospects of improvement.

**Remarks and caveats** We did not include latitude dependent effects, such as the limited time to observe a source (discussed in the last section) or the absorption in the Earth, in order to simplify the discussion. The latter effect is more severe for the fluxes that extend up to the highest energies, namely those with a smaller value of  $\alpha$  and/or a higher energy cutoff. We roughly take into account this, by limiting the spectrum to  $E_\nu < 1$  PeV.

Let us repeat that the  $\gamma$ -ray data permit us to obtain an upper bound on neutrinos, postulating that the source is transparent to its  $\gamma$ -rays. But in some cases, high energy neutrinos and  $\gamma$ -rays do not correlate. This is thought to happen for certain interesting astrophysical objects such as galactic binary systems containing a luminous optical star and a compact object (microquasars) where the absorption of  $\gamma$ -rays is considerable. Cases like this increase the *a priori* chance of having surprisingly large neutrino fluxes. At

---

<sup>2</sup>A useful resource is the HESS Source Catalog that can be consulted at: <http://www.mpi-hd.mpg.de/hfm/HESS/pages/home/sources/>.

the same time, such a situation causes further difficulties to obtain reliable expectations, due to the increased dependence on an uncertain theoretical modelling. For a more complete discussion of alternative galactic neutrino sources, see **Aharonian** (2007).

### 5.3 Toward reliable predictions for the SNR RX J1713.7-3946

In this section we analyze why supernova remnants are expected to act as emitters of high energy neutrinos and discuss in details the promising case of the supernova remnant called RX J1713.7-3946. The kinetic energy of supernova remnants (SNR) is one order of magnitude larger than the cosmic ray losses of the Galaxy (Ginzburg and Syrovatskii (1964)) and diffusive acceleration on the shock wave (Fermi (1949)) can provide the mechanism for cosmic-ray acceleration (see e.g., Malkov and O’C Drury (2001)): Thus, we expect that SNR’s contain high densities of cosmic rays. The SNR can also be sources of high energy  $\gamma$ -rays and neutrinos, especially when they are associated with molecular clouds, that act as a target for the cosmic ray collisions (**Aharonian** et al. (1994), Drury et al. (1994)). The spectrum of the young SNR RX J1713.7-3946, measured by HESS (**Aharonian** et al. (2007b)) till 100 TeV and (as already discussed) exceeding the bound of Eq. 5.2.2, has a special interest in the discussion of high energy neutrinos. This is even more true when one realizes that this SNR interacts with a system of molecular clouds detected by NANTEN (Fukui et al. (2003), Sano et al. (2010)). It is in the Southern neutrino sky, relatively close to us,  $D \sim 1$  kpc.

These are the reasons why it is urgent to ask: How far we are from understanding the high energy neutrinos of *this* SNR? To address this question, we have to consolidate the physical picture of RX J1713.7-3946, that can be done only employing in the best way the available (theoretical and observational) information.

**A model for the spectrum** A related question that we should tackle is which is the nature of the electromagnetic spectrum of RX J1713.7-3946. There are various models in the literature, e.g., Malkov et al. (2005), Berezhko and Völk (2010), Morlino et al. (2009), Zirakashvili and **Aharonian** (2010), Ellison et al. (2010), Fan et al. (2010). In a typical model, the  $\gamma$ -ray emission is dominated by a single mechanism at all energies, which reduces the question of neutrinos to a dichotomy.

We focus on one proposal of Zirakashvili and **Aharonian** (2010), where the spectrum is instead composite: it has significant contributions both from the Inverse Compton (IC, i.e. leptonic mechanism) and from neutral pion decays ( $\pi^0$ , i.e. hadronic mechanism). Even if their model will turn out to be incorrect

Energy of $\gamma$ -rays	Dominant emission	Observational test	Relevant data
$\sim 1-10$ GeV	$\pi^0$	intensity & shape	Fermi, Agile
$\sim 1-10$ TeV	IC	SNR shell	HESS
$> 10$ TeV	$\pi^0$	molecular clouds	HESS

**Table 5.2:** Tests of the Zirakashvili & Aharonian model for the  $\gamma$ -ray spectrum of the SNR named RX J1713.7-3946. First column, the energy range of the measurement; second, the dominant mechanism of emission expected in the model; third, the possible test; last column, the relevant experiment. See the text for details.

in some quantitative aspect, such a hypothesis allows us to make one step ahead in the right direction: to understand neutrinos, we need to know *which part* of the  $\gamma$ -ray emission is hadronic.

This proposal has good physical motivations: 1) The similarity of the features observed in X-rays is explained, since the IC dominates the integrated spectrum measured by HESS. 2) Attributing the high energy tail of the spectrum to  $\pi^0$  decays instead overcomes the difficulties in accounting for it by IC, whose spectrum should be cut-off abruptly. The question we want to address becomes: How do we test the predictions of this model?

**Prospects of observational tests** The measurements of Agile and Fermi in the energy range 1-10 GeV will be a key test (see e.g., Morlino et al. (2009)), for the shape of the  $\gamma$ -ray spectrum at GeV energies depends on the mechanism of emission: Assuming that protons and electrons have power-law spectra with the same slope,  $\propto E_{p,e}^{-\alpha}$ ,  $\pi^0$  decays give  $\propto E_{\gamma}^{-(\alpha-0.1)}$  whereas IC gives  $\propto E_{\gamma}^{-(\alpha+1)/2}$ ; thus, extrapolating the  $\gamma$ -ray spectra from the lowest point measured by HESS,  $E_{\gamma} = 300$  GeV, we find that the hadronic mechanism leads to an emission 3 times more intense than the one due to the leptonic mechanism already at 10 GeV. But it is unclear whether Agile or Fermi will attain sufficient angular resolution to reveal that the  $\gamma$ -rays come preferentially from the sites where cosmic ray collisions and  $\pi^0$  decays are more frequent, i.e. the molecular clouds.

This qualifying hypothesis could be verifiable at much larger energies. In fact, the model of Zirakashvili and Aharonian (2010) predicts, at several tens of TeV, a  $\gamma$ -ray signal enhanced in the direction of the overdense molecular clouds of NANTEN, of size  $(2-8) \mu\text{sr}$  Sano et al. (2010)), on top of the known background distribution due to misidentified cosmic rays and of a minor component of the signal distributed as the SNR shell.

Do we have enough data to test this picture? HESS (Aharonian et al. (2007b)) has 1021 (resp., 474) events ON against 751 (resp., 338) OFF above 20 (resp., 30) TeV, namely about 250 (resp., 130) signal events<sup>3</sup>. To illustrate the mean-

---

<sup>3</sup>The terminology ON/OFF refers to the two cases when the gamma ray telescope points to

ing of these numbers, suppose that 750 background events are uniformly distributed in 25 patches of equal area; thus, 30 signal events in a single patch are enough to double the average density of events. The low statistics conditions suggest an unbinned likelihood analysis of the  $\gamma$ -ray data, as those proposed for similar applications in neutrino astronomy by Braun et al. (2008) and by Ianni et al. (2009).

A résumé of possible tests is provided in Tab 5.2.

The above estimates show that the existing HESS data can only marginally provide a decisive study of energy dependent  $\gamma$ -ray morphology of RX J1713.7-3946. Thus, it is highly desirable to increase significantly the TeV photon statistics by new observations of the source. Presently such observations can be performed only by the HESS array of telescopes. However, because of the limited potential of HESS at energies above 10 TeV, we can hope for enhancement of photon statistics, for any reasonable observation time, only by a factor of two or so. A real breakthrough in this regard is expected only with the next generation  $\gamma$ -ray instruments like CTA.

**Implications for high energy neutrino astronomy** If the model of Zirakashvili & Aharonian will be validated by future data analyses, the induced muon flux from RX J1713.7-3946 will be lower than the upper limit that we derive in the extreme hypothesis of hadronic emission from Eq. 5.2.3, namely:  $I_{\mu+\bar{\mu}}(> 1 \text{ TeV}) < 3.5 / (\text{km}^2 \text{ yr})$  at 90 % CL. This will make the search for a signal more difficult but will be accompanied by a decrease of the background, for the sources of high energy neutrinos are the relatively small molecular clouds and not the much larger SNR.

By comparing the size of the overdense clouds with the one of the SNR, one would expect in ideal conditions a decrease of the background by a factor of ten; however, the decrease will be limited by instrumental features, if the angular resolution of the neutrino telescopes will be larger than the cloud size. Just for illustration, an angular resolution of  $\delta\theta = 0.2^\circ$  at the relevant energies corresponds to a search window of  $\pi \delta\theta^2 = 40 \mu\text{sr}$ . Multiplying by the number of the main overdense clouds, i.e. four (see Sano et al. (2010)) and comparing to the size of the SNR implies a decrease of the background by a factor of two.

We would like to emphasize that the model of Zirakashvili and Aharonian (2010) does not necessarily imply a strong reduction of the neutrino detection rate compared to the pure hadronic model, because in the composite spectrum the most relevant  $\gamma$ -rays—those with energy above 10 TeV—are contributed mainly by cosmic ray interactions. On the other hand, the composite model implies that the  $\gamma$ -rays and of course the high energy neutrinos are produced in more compact regions, which leads to a significant reduction of background events.

---

the source and when instead it points to a region where no signal is expected.

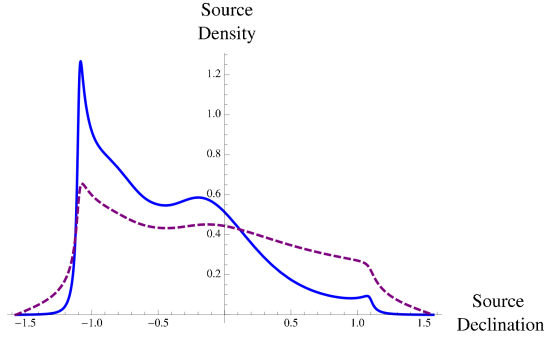


**Figure 5.2:** *Continuous line: normalized mass distribution of the Galaxy, as a function of the declination. Dashed line, the same but weighted with the inverse squared distance from the mass.*

We will be in a better position to quantify the expected, neutrino-induced muon flux when we will know the results of the analyses of Agile and Fermi. In order to predict the very high-energy neutrino flux, it would be even more important to know the amount of very high-energy  $\gamma$ -rays correlated with the molecular clouds. HESS could provide us with some evidence for such a hadronic emission, but future high statistics observations will be crucial to obtain reliable measurements (or strong limits) of this component of the  $\gamma$ -ray emission.

## 5.4 An appraisal of a telescope in the Northern Hemisphere

In the last section, we discuss the importance of operating a new telescope for high energy neutrinos in the Northern Hemisphere. The discussion elaborates quantitatively the oft-heard observation: most of the Galaxy, being in the Southern Hemisphere, lies in the Northern neutrino sky. We begin by considering an educated guess on the galactic sources of neutrinos. It is plausible that the distribution of neutrino sources follows the mass distribution of supernovae, young matter and/or star-forming regions. We use the distribution of neutron stars of Yusifov and Küçük (2004), adopted for the study of supernova neutrinos of Mirizzi et al. (2006) (see their Eqs. (1), (2) and (4) and compare with Costantini et al. (2005)). We set the  $x$ -axis from the galactic center to the Earth, the  $z$ -axis in the direction of the galactic North, obtaining for components of the Earth's rotation axis the unit vector  $(u_x, u_y, u_z) = (.484, .747, .456)$ .

Now we derive the normalized mass distribution as a function of the declination of the sources  $\delta$ , that we regard as the probability of finding neutrino sources. Similarly, we derive the mass distribution weighted with the inverse

of the squared distance of the source, accounting for the fact that the number of events scales as  $1/r^2$  for a standard source. The results are given in Figure 5.2 and are easy to understand: The angle between the galactic plane and the Celestial equator is  $\sim \pi/3$ , thus most of the matter is at  $|\delta| < 1$ ; furthermore, the galactic center is at  $\delta \sim -\pi/6$ , thus the region  $\delta < 0$  is more populated; finally, the features are less prominent when we include  $1/r^2$  since this emphasizes the local patch of the Galaxy rather than the distant regions.

Let us consider the traditional signal of induced muons. High energy neutrino detectors observe only downward to safely avoid atmospheric muons; thus, a source at declination  $\delta$  is seen only for a fraction of time:

$$f[\delta, \phi] = 1 - \frac{\text{Re}[\arccos(-\tan \delta \tan \phi)]}{\pi} \quad (5.4.1)$$

as a function of the latitude  $\phi$  of the detector, as discussed e.g., in Costantini et al. (2005). For instance, the galactic center, that is in the Southern sky at  $\delta = -29^\circ$ , is invisible in IceCube ( $f = 0$ ) and it is seen for a fraction of time  $f = 67\%$ ,  $63\%$ ,  $64\%$  or  $75\%$  in Antares, NEMO, Nestor or Baikal respectively.

By convoluting  $f$  with the distribution of the matter in the Milky Way we estimate the relevance of a high energy neutrino detector. The result is shown in the curves Figure 5.3. They are symmetric around  $1/2$  when  $\phi \rightarrow -\phi$ , just as  $f$ :  $f[\delta, \phi] + f[\delta, -\phi] = 1$ , for two antipodal detectors see the entire sky. From this figure, we verify that the South Pole is a less promising place to search for neutrinos from galactic sources. A detector in the Mediterranean, say with latitude  $\phi = 36^\circ 30'$ , has 2.9 times better chances; when we weight the mass distribution with  $1/r^2$ , the improvement is a factor of 1.4 instead. The first number applies if the hypothetical sources are so intense, that all of them can be seen; the second one is plausibly a better estimation of the factor of improvement if there is a sort of “standard source” with a fixed intensity, and the neutrino detectors are able to see only the closest ones.

Similar arguments are frequently invoked in favor of a detector in the Northern hemisphere; however, the quantitative evaluation of the factor of improvement that we obtained is, to the best of our knowledge, a new result.

**Remarks and caveats** There are other aspects to be kept in mind; e.g., it seems possible to cover safely a few degrees above the horizon already with IceCube (Abbasi et al. (2009)). Also, when KM3NeT will operate, a portion of the sky will be already explored by IceCube; however, some redundancy in the observations could be precious to cross check the proper functioning of the detectors.

One can repeat the calculations including the halo, or a “bar” as part of the Milky Way, possibilities that above we disregarded. Alternatively, one could consider suitable generalizations, for instance the case of dark matter decay or annihilation; the latter requires to weight the fraction  $f$  with the square

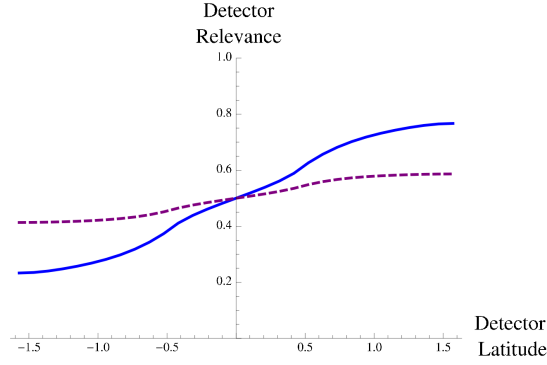


**Figure 5.3:** Fraction of the Galaxy seen by a neutrino detector at a given latitude. For the dashed lines, the mass distribution was weighted with  $1/r^2$  to take into account that nearby sources are easier to detect.

of the density of the dark matter distribution. Many of these cases resemble closely a source in the galactic center, discussed above.

## 5.5 Summary and discussion

The discovery of sources of high energy neutrinos is a well-recognized scientific goal: The hunt has been opened by IceCube and will be complemented by KM3NeT, see Anchordoqui and Montaruli (2010) for reviews. However, we cannot rely on precise predictions yet. Clear expectations would be helpful or even necessary to focus the search and to optimize the new instruments: their area, geometry, energy threshold, etc.. The precise upper bounds that we can derive from  $\gamma$ -ray data are useful, but insufficient for these aims. With these considerations in mind, we made an effort to determine some of the boundaries of the present knowledge and to discuss the prospects to proceed toward definite expectations, focussing on the main target of KM3NeT: galactic neutrino sources.

A new high-energy neutrino telescope in the Northern Hemisphere is considered highly desirable. We discussed in Sec. 5.2 which  $\gamma$ -ray sources may yield a minimum signal in neutrino telescopes, assuming that the  $\gamma$ -rays are not absorbed. We found that, for high energy neutrino search, it would be particularly important to know the  $\gamma$ -ray sources with a sufficiently intense emission around 20 TeV: see Eq. 5.2.2. We argued in Sec. 5.3 that there are reasonable chances of getting a reliable prediction for RX J1713.7-3946, that could become a reference target for a telescope located in the Northern hemisphere. The chances are linked to future analyses of existing  $\gamma$ -ray data: those by Agile and Fermi, which should reveal an emission more intense than the one expected assuming the leptonic mechanism; those by HESS above 20 – 30 TeV, that should reveal the correlation of the  $\gamma$ -ray events with the molecular

clouds that interact with RX J1713.7-3946. Finally, we discussed the importance to have a new high-energy neutrino telescope in the Northern Hemisphere. We developed in Sec. 5.4 the oft-heard argument in favor of such an instrument, concluding that it will be superior by a factor of 1.4-2.9 to Ice-Cube as a monitor of galactic neutrino sources distributed as the matter of the Milky Way.



## 6 Future plans related to the Byurakan Observatory

We plan to involve the Byurakan Observatory in the future activity of the Yerevan seat of ICRA Net. One of the projects could be the use of the 2.6m telescope for multiwavelength studies of the short, burst-type high energy phenomena, especially for detection of afterglows of Gamma Ray Burst (GRBs). The study of the physics and astrophysics of GRBs is one of the highest priorities of the research of ICRA Net and will be in the focus of interests of the Yerevan group. This telescope can be effectively used also for coordinated multiwavelength campaigns for studies of gamma-ray flares of AGN and microquasars. In this regard, the use of 2.6m telescope and possibly some other instruments (in particular the 1m diameter Schmidt telescope) as complementary tools for study of high energy transient phenomena, could be considered as a natural involvement of the Byurakan observatory in the activity of the Yerevan group.

For successful realization of such a project, the Byurakan observatory should provide adequate infrastructure and man power.



# Bibliography

- ABBASI, R., ABDOU, Y., ACKERMANN ET AL.  
«First Neutrino Point-Source Results from the 22 String Icecube Detector».  
*ApJL*, **701**, pp. L47–L51 (2009).
- ABDO, A.A., ACKERMANN, M., AJELLO, M. ET AL.  
«Fermi Gamma-Ray Imaging of a Radio Galaxy».  
*Science*, **328**, pp. 725– (2010a).
- ABDO, A.A., ACKERMANN, M., AJELLO, M. ET AL.  
«Fermi Large Area Telescope View of the Core of the Radio Galaxy Centaurus A».  
*ApJ*, **719**, pp. 1433–1444 (2010b).
- AHARONIAN, T.  
«Galactic Sources of High Energy Neutrinos».  
*ArXiv Astrophysics e-prints* (2007).
- AHARONIAN, T., AKHPERJANIAN, A.G., ANTON, G. ET AL.  
«H.E.S.S. Observations of the Supernova Remnant RX J0852.0-4622: Shell-Type Morphology and Spectrum of a Widely Extended Very High Energy Gamma-Ray Source».  
*ApJ*, **661**, pp. 236–249 (2007a).
- AHARONIAN, T., AKHPERJANIAN, A.G., ANTON, G. ET AL.  
«Primary particle acceleration above 100 TeV in the shell-type supernova remnant RX J1713.7-3946 with deep HESS observations».  
*A&A*, **464**, pp. 235–243 (2007b).
- AHARONIAN, T., AKHPERJANIAN, A.G., ANTON, G. ET AL.  
«Discovery of Very High Energy  $\gamma$ -Ray Emission from Centaurus a with H.E.S.S.»  
*ApJL*, **695**, pp. L40–L44 (2009).
- AHARONIAN, T. AND ATOYAN, A.M.  
«Compton scattering of relativistic electrons in compact X-ray sources».  
*Ap&SS*, **79**, pp. 321–336 (1981).
- AHARONIAN, T., DRURY, L.O. AND VOELK, H.J.  
«GeV/TeV gamma-ray emission from dense molecular clouds overtaken by supernova shells».

- A&A*, **285**, pp. 645–647 (1994).
- ALVAREZ, H., APARICI, J., MAY, J. AND REICH, P.  
«The radio continuum spectrum of Centaurus A's large-scale components».  
*A&A*, **355**, pp. 863–872 (2000).
- ANCHORDOQUI, L.A. AND MONTARULI, T.  
«In Search of Extraterrestrial High-Energy Neutrinos».  
*Annual Review of Nuclear and Particle Science*, **60**, pp. 129–162 (2010).
- ATOYAN, A.M. AND AHARONIAN, T.  
«Modelling of the non-thermal flares in the Galactic microquasar GRS 1915+105».  
*MNRAS*, **302**, pp. 253–276 (1999).
- ATWOOD, W.B., ABDO, A.A., ACKERMANN, M. ET AL.  
«The Large Area Telescope on the Fermi Gamma-Ray Space Telescope Mission».  
*ApJ*, **697**, pp. 1071–1102 (2009).
- BEREZHKO, E.G. AND VÖLK, H.J.  
«Nonthermal and thermal emission from the supernova remnant RX J1713.7-3946».  
*A&A*, **511**, A34 (2010).
- BRAUN, J., DUMM, J., DE PALMA, F., FINLEY, C., KARLE, A. AND MONTARULI, T.  
«Methods for point source analysis in high energy neutrino telescopes».  
*Astroparticle Physics*, **29**, pp. 299–305 (2008).
- CAPPELLARI, M., NEUMAYER, N., REUNANEN, J., VAN DER WERF, P.P., DE ZEEUW, P.T. AND RIX, H.W.  
«The mass of the black hole in Centaurus A from SINFONI AO-assisted integral-field observations of stellar kinematics».  
*MNRAS*, **394**, pp. 660–674 (2009).
- CHIABERGE, M., CAPETTI, A. AND CELOTTI, A.  
«The BL Lac heart of Centaurus A».  
*MNRAS*, **324**, pp. L33–L37 (2001).
- COSTANTINI, M.L., IANNI, A. AND VISSANI, F.  
«The interest in neutrinos from core collapse supernovae».  
*Nuclear Physics B Proceedings Supplements*, **139**, pp. 27–32 (2005).
- CROSTON, J.H., KRAFT, R.P., HARDCASTLE, M.J. ET AL.

- «High-energy particle acceleration at the radio-lobe shock of Centaurus A».  
*MNRAS*, **395**, pp. 1999–2012 (2009).
- DRURY, L.O., AHARONIAN, T. AND VOELK, H.J.  
«The gamma-ray visibility of supernova remnants. A test of cosmic ray origin».  
*A&A*, **287**, pp. 959–971 (1994).
- ELLISON, D.C., PATNAUDE, D.J., SLANE, P. AND RAYMOND, J.  
«Efficient Cosmic Ray Acceleration, Hydrodynamics, and Self-Consistent Thermal X-Ray Emission Applied to Supernova Remnant RX J1713.7-3946».  
*ApJ*, **712**, pp. 287–293 (2010).
- FAN, Z.H., LIU, S.M., YUAN, Q. AND FLETCHER, L.  
«Lepton models for TeV emission from SNR RX J1713.7-3946».  
*A&A*, **517**, L4 (2010).
- FANAROFF, B.L. AND RILEY, J.M.  
«The morphology of extragalactic radio sources of high and low luminosity».  
*MNRAS*, **167**, pp. 31P–36P (1974).
- FEAIN, I.J., CORNWELL, T.J., EKERS, R.D. ET AL.  
«The Radio Continuum Structure of Centaurus A at 1.4 GHz».  
*ApJ*, **740**, 17 (2011).
- FEAIN, I.J., EKERS, R.D., MURPHY, T. ET AL.  
«Faraday Rotation Structure on Kiloparsec Scales in the Radio Lobes of Centaurus A».  
*ApJ*, **707**, pp. 114–125 (2009).
- FERMI, E.  
«On the Origin of the Cosmic Radiation».  
*Physical Review*, **75**, pp. 1169–1174 (1949).
- FRANCESCHINI, A., RODIGHIERO, G. AND VACCARI, M.  
«Extragalactic optical-infrared background radiation, its time evolution and the cosmic photon-photon opacity».  
*A&A*, **487**, pp. 837–852 (2008).
- FUKUI, Y., MORIGUCHI, Y., TAMURA, K. ET AL.  
«Discovery of Interacting Molecular Gas toward the TeV Gamma-Ray Peak of the SNR G 347.3–0.5».  
*PASJ*, **55**, pp. L61–L64 (2003).

- GINZBURG, V.L. AND SYROVATSKII, S.I.  
*The Origin of Cosmic Rays* (1964).
- HARDCASTLE, M.J., CHEUNG, C.C., FEAIN, I.J. AND STAWARZ, Ł.  
«High-energy particle acceleration and production of ultra-high-energy cosmic rays in the giant lobes of Centaurus A».  
*MNRAS*, **393**, pp. 1041–1053 (2009).
- HARDCASTLE, M.J. AND CROSTON, J.H.  
«Modelling TeV  $\gamma$ -ray emission from the kiloparsec-scale jets of Centaurus A and M87».  
*MNRAS*, **415**, pp. 133–142 (2011).
- HARDCASTLE, M.J., WORRALL, D.M., KRAFT, R.P., FORMAN, W.R., JONES, C. AND MURRAY, S.S.  
«Radio and X-Ray Observations of the Jet in Centaurus A».  
*ApJ*, **593**, pp. 169–183 (2003).
- HARTMAN, R.C., BERTSCH, D.L. AND BLOOM, S.D.  
«The Third EGRET Catalog of High-Energy Gamma-Ray Sources».  
*ApJSS*, **123**, pp. 79–202 (1999).
- IANNI, A., PAGLIAROLI, G., STRUMIA, A., TORRES, F.R., VILLANTE, F.L. AND VISSANI, F.  
«Likelihood for supernova neutrino analyses».  
*Phys. Rev. D*, **80(4)**, 043007 (2009).
- ISOBE, N., MAKISHIMA, K., TASHIRO, M. AND KANEDA, H.  
«ASCA observations of the northern outer lobe edge of the radio galaxy Centaurus A».  
In R.A. Laing and K.M. Blundell (eds.), *Particles and Fields in Radio Galaxies Conference*, volume 250 of *Astronomical Society of the Pacific Conference Series*, p. 394 (2001).
- ISRAEL, F.P.  
«Centaurus A - NGC 5128».  
*A&AR*, **8**, pp. 237–278 (1998).
- KACHELRIESS, M., OSTAPCHENKO, S. AND TOMÀS, R.  
«TeV Gamma Rays from Ultrahigh Energy Cosmic Ray Interactions in the Cores of Active Galactic Nuclei: Lessons from Centaurus A».  
*PASA*, **27**, pp. 482–489 (2010).
- KAPPES, A., HINTON, J., STEGMANN, C. AND AHARONIAN, T.  
«Potential Neutrino Signals from Galactic  $\gamma$ -Ray Sources».  
*ApJ*, **656**, pp. 870–878 (2007).

- KRAFT, R.P., FORMAN, W.R., JONES, C., MURRAY, S.S., HARDCASTLE, M.J. AND WORRALL, D.M.  
«Chandra Observations of the X-Ray Jet in Centaurus A».  
*ApJ*, **569**, pp. 54–71 (2002).
- LENAIN, J.P., BOISSON, C., SOL, H. AND KATARZYŃSKI, K.  
«A synchrotron self-Compton scenario for the very high energy  $\gamma$ -ray emission of the radiogalaxy M 87. Unifying the TeV emission of blazars and other AGNs?»  
*A&A*, **478**, pp. 111–120 (2008).
- LIPARI, P.  
«Perspectives of high-energy neutrino astronomy».  
*Nuclear Instruments and Methods in Physics Research A*, **567**, pp. 405–417 (2006).
- MA, C., ARIAS, E.F., EUBANKS, T.M. ET AL.  
«The International Celestial Reference Frame as Realized by Very Long Baseline Interferometry».  
*AJ*, **116**, pp. 516–546 (1998).
- MALKOV, M.A., DIAMOND, P.H. AND SAGDEEV, R.Z.  
«On the Gamma-Ray Spectra Radiated by Protons Accelerated in Supernova Remnant Shocks near Molecular Clouds: The case of Supernova Remnant RX J1713.7-3946».  
*ApJL*, **624**, pp. L37–L40 (2005).
- MALKOV, M.A. AND O’C DRURY, L.  
«Nonlinear theory of diffusive acceleration of particles by shock waves».  
*Reports on Progress in Physics*, **64**, pp. 429–481 (2001).
- MARCONI, A., PASTORINI, G., PACINI, F., AXON, D.J., CAPETTI, A., MACCHETTO, D., KOEKEMOER, A.M. AND SCHREIER, E.J.  
«The supermassive black hole in Centaurus A: a benchmark for gas kinematical measurements».  
*A&A*, **448**, pp. 921–953 (2006).
- MEISENHEIMER, K., TRISTRAM, K.R.W., JAFFE, W. ET AL.  
«Resolving the innermost parsec of Centaurus A at mid-infrared wavelengths».  
*A&A*, **471**, pp. 453–465 (2007).
- MIRIZZI, A., RAFFELT, G.G. AND SERPICO, P.D.  
«Earth matter effects in supernova neutrinos: optimal detector locations».  
*JCAP*, **5**, 012 (2006).

- MORGANTI, R., FOSBURY, R.A.E., HOOK, R.N., ROBINSON, A. AND TSVE-  
TANOV, Z.  
«Evidence for a BL Lac nucleus in Centaurus A».  
*MNRAS*, **256**, pp. 1P–5P (1992).
- MORLINO, G., BLASI, P. AND AMATO, E.  
«Gamma rays and neutrinos from SNR RX J1713.7-3946».  
*Astroparticle Physics*, **31**, pp. 376–382 (2009).
- MÜLLER, C., KADLER, M., OJHA, R. ET AL.  
«Dual-frequency VLBI study of Centaurus A on sub-parsec scales. The  
highest-resolution view of an extragalactic jet».  
*A&A*, **530**, L11 (2011).
- NOLAN, P.L., ABDO, A.A., ACKERMANN, M., AJELLO, M., ALLAFORT, A.,  
ANTOLINI, E., ATWOOD, W.B., AXELSSON, M., BALDINI, L., BALLEST, J.  
ET AL.  
«Fermi Large Area Telescope Second Source Catalog».  
*ApJSS*, **199**, 31 (2012).
- O’SULLIVAN, S., REVILLE, B. AND TAYLOR, A.M.  
«Stochastic particle acceleration in the lobes of giant radio galaxies».  
*MNRAS*, **400**, pp. 248–257 (2009).
- RIEGER, F.M.  
«Nonthermal Processes in Black Hole-Jet Magnetospheres».  
*International Journal of Modern Physics D*, **20**, pp. 1547–1596 (2011).
- RIEGER, F.M. AND AHARONIAN, T.  
«Centaurus A as TeV  $\gamma$ -ray and possible UHE cosmic-ray source».  
*A&A*, **506**, pp. L41–L44 (2009).
- ROUSTAZADEH, P. AND BÖTTCHER, M.  
«Very High Energy Gamma-ray-induced Pair Cascades in the Radiation  
Fields of Dust Tori of Active Galactic Nuclei: Application to Cen A».  
*ApJ*, **728**, 134 (2011).
- SAHU, S., ZHANG, B. AND FRAIJA, N.  
«Hadronic-origin TeV  $\gamma$  rays and ultrahigh energy cosmic rays from Cen-  
taurus A».  
*Phys. Rev. D*, **85(4)**, 043012 (2012).
- SANO, H., SATO, J., HORACHI, H. ET AL.  
«Star-forming Dense Cloud Cores in the TeV Gamma-ray SNR RX J1713.7-  
3946».  
*ApJ*, **724**, pp. 59–68 (2010).

- SREEKUMAR, P., BERTSCH, D.L., HARTMAN, R.C., NOLAN, P.L. AND THOMPSON, D.J.  
«GeV emission from the nearby radio galaxy Centaurus A».  
*Astroparticle Physics*, **11**, pp. 221–223 (1999).
- STAWARZ, Ł., AHARONIAN, T., WAGNER, S. AND OSTROWSKI, M.  
«Absorption of nuclear  $\gamma$ -rays on the starlight radiation in FR I sources: the case of Centaurus A».  
*MNRAS*, **371**, pp. 1705–1716 (2006).
- STEINLE, H., BENNETT, K., BLOEMEN, H., COLLMAR, W., DIEHL, R., HERMSEN, W., LICHTI, G.G., MORRIS, D., SCHONFELDER, V., STRONG, A.W. ET AL.  
«COMPTEL observations of Centaurus A at MeV energies in the years 1991 to 1995».  
*A&A*, **330**, pp. 97–107 (1998).
- SU, M., SLATYER, T.R. AND FINKBEINER, D.P.  
«Giant Gamma-ray Bubbles from Fermi-LAT: Active Galactic Nucleus Activity or Bipolar Galactic Wind?»  
*ApJ*, **724**, pp. 1044–1082 (2010).
- TINGAY, S.J., JAUNCEY, D.L., REYNOLDS, J.E. ET AL.  
«The Subparsec-Scale Structure and Evolution of Centaurus A: The Nearest Active Radio Galaxy».  
*AJ*, **115**, pp. 960–974 (1998).
- VAN DER WOLK, G., BARTHEL, P.D., PELETIER, R.F. AND PEL, J.W.  
«Dust tori in radio galaxies».  
*A&A*, **511**, A64 (2010).
- VILLANTE, F.L. AND VISSANI, F.  
«Method to extract the primary cosmic ray spectrum from very high energy  $\gamma$ -ray data and its application to SNR RX J1713.7-3946».  
*Phys. Rev. D*, **76(12)**, 125019 (2007).
- VILLANTE, F.L. AND VISSANI, F.  
«How precisely can neutrino emission from supernova remnants be constrained by gamma ray observations?»  
*Phys. Rev. D*, **78(10)**, 103007 (2008).
- VISSANI, F.  
«Neutrinos from galactic sources of cosmic rays with known  $\gamma$ -ray spectra».  
*Astroparticle Physics*, **26**, pp. 310–313 (2006).

YANG, R.Z., SAHAKYAN, T., DE ONA WILHELMI, E., AHARONIAN, T. AND RIEGER, F.

«Deep observation of the giant radio lobes of Centaurus A with the Fermi Large Area Telescope».

*A&A*, **542**, A19 (2012).

YUSIFOV, I. AND KÜÇÜK, I.

«Revisiting the radial distribution of pulsars in the Galaxy».

*A&A*, **422**, pp. 545–553 (2004).

ZIRAKASHVILI, V.N. AND AHARONIAN, T.

«Nonthermal Radiation of Young Supernova Remnants: The Case of RX J1713.7-3946».

*ApJ*, **708**, pp. 965–980 (2010).